MEASUREMENT & INVESTIGATION OF ADIABATIC SHEAR BANDING-INDUCED TI-6AL-4V CHIP MORPHOLOGY & PROCESS CHARACTERISTICS

An Undergraduate Research Scholars Thesis

by

EVAN LOEHR

Submitted to the Undergraduate Research Scholars program at
Texas A&M University
in partial fulfillment of the requirements for the designation as an

UNDERGRADUATE RESEARCH SCHOLAR

Approved by Research Advisor: Dr. Mathew Kuttolamadom

May 2018

Major: Manufacturing & Mechanical Engineering Technology

TABLE OF CONTENTS

ABSTRACT

Measurement & Investigation of Adiabatic Shear Banding-Induced Ti-6Al-4V Chip Morphology & Process Characteristics

Evan Loehr
Department of Engineering Technology & Industrial Distribution
Texas A&M University

Research Advisor: Dr. Mathew Kuttolamadom
Department of Engineering Technology & Industrial Distribution
Department of Materials Science & Engineering
Texas A&M University

The research objective of this project is to measure and investigate the ultra-high frequency aspects of adiabatic shear banding (ASB) during the Ti-6Al-4V chip generation process through the use of a piezoelectric-based dynamometer and accelerometer-based multi-directional force and acceleration sensing systems. For this, a coupled force-acceleration measurement system will be first assembled and calibrated. Then, an experimental design of machining tests will be conducted to elucidate the relationships between ASB-induced machining force/acceleration components and the resulting chip morphology and process characteristics. This understanding is expected to help generate strategies to control ASB geometry and characteristics by suitably altering the process parameters such as machining speed, feed and cutting depth. These will be validated through further machining tests to show productivity improvements.

ACKNOWLEDGEMENTS

I would like to thank my undergraduate research advisor, Dr. Mathew Kuttolamadom, for allowing me to conduct this research. His guidance and expertise have helped me to understand new concepts quickly and accomplish great work in a short time. This was a wonderful experience and I am thankful to have had this opportunity.

I would also like to thank Texas A&M University and its faculty members who were always willing to lend help or resources whenever possible, especially Laxmi Sai Prasad without whom this work would not have been complete. This experience will be useful in my remaining time as a student, as well as my future career after graduation.

NOMENCLATURE

A	Area
a_1	Segment Spacing
a_2	Saw-Tooth Height
a_3	Continuous Portion Height
ASB	Adiabatic Shear Banding
DAQ	Data Acquisition System
DOE	Design of Experiments
F	Force
f	Feed Rate (inch/revolution)
FFT	Fast Fourier Transform
h	Half Shear Band Width
ID	Inner Diameter
Lc	Shear Band Spacing
M	Mass
MEMS	Micro-Electro-Mechanical Systems
OD	Outer Diameter
RCD	Rotating dynamometers
S	Relative surface speed between tool and workpiece surface
θ_1	Crack Initiation Angle
θ_2	Saw-Tooth Included Angle

CHAPTER I

INTRODUCTION

Introduction

Titanium and its alloys are widely used in critical structural and other functional applications in the aerospace field due to its high strength-to-weight ratio and its ability to maintain strength even under high temperatures, as well as in the biomedical field because of its excellent corrosion resistance and biocompatibility[1–4]. Among the various manufacturing processes used for fabricating titanium alloy components, one of the most common methods include machining (e.g., operations such as milling, turning, drilling, etc.). However, it is challenging to machine many of the common titanium alloys and especially the workhorse titanium alloy, Ti-6Al-4V predominantly because of its combination of high-temperature strength and low thermal conductivity which leads to very high temperatures resulting in unpredictable and catastrophic wear/damage to the machining tool/insert[3].

Among the numerous tool/workpiece/process condition monitoring parameters, the evolving chip morphologies in Ti-6Al-4V machining is an important characteristic to track due to the fact that the chip formation process has a direct impact on the accuracy and surface state of the final work piece, as well as the usable lifespan of the tool[3]. In certain titanium alloys (such as in Ti-6Al-4V), the chip formation is often characterized by cyclic localization of the plastic flow in the form of adiabatic shear bands (ASB) which create a “saw-tooth” like chip pattern caused by catastrophic thermoplastic shear[1,3–8]. The serration pattern occurs due to a phenomenon known as adiabatic shear, where the low thermal conductivity of the material aids in high-strain

high-rate shear of the material during the chip generation process. This phenomenon occurs due to the fact that the rate of loss of strength caused by the local increase in temperature is equal to or (usually) greater that the rate of increase in strength caused by strain hardening in the affected shear zone[2,4]. As the chips are created, excessive heat builds up at the tool-chip interface, however the heat is not able to dissipate to a new plane (due to the low thermal conductivity of the material) and therefore cooler material is plastically deformed around the cut and sheared, which causes the characteristic saw-tooth chip. Chip morphology and the formation/extent of adiabatic shear banding tend to vary in accordance with the cutting conditions, often leading to significant vibrations and force fluctuations during the machining process. These vibrations are due to the chip segmentation process that limits material removal rates. Thus, in order to be able to increase both productivity and tool life in regard to the machining of certain titanium alloys (especially the workhorse alloy, Ti-6Al-4V), it is necessary to study the high-frequency forces and the mechanics of chip segmentation.[8]

Chip formation in Ti-6Al-4V typically involves two separate fracture mechanisms: first a "ductile fracture mechanism"[3] caused by strain under compressive stress, and second, a "high speed ductile fracture mechanism"[3] caused by a concentrated strain due to local thermal weakening. Adverse effects of shear banding include large oscillations in forces and other fluctuations at the tool-chip-workpiece interfaces[5]. This results in poor tool life due to high stress and fatigue as well as a loss in the homogeneity of key workpiece characteristics such as surface finish and surface/sub-surface microstructure[9].

The short time scales in which these shear bands are generated (often in the order of tens of microseconds) makes direct experimental observations rather difficult. Thus, an advancement in the equipment capabilities for high-speed measurement of shear band characteristics and the associated force/acceleration signatures will lead to an improved understanding of the instability phenomena in machining and possible methods for their control for productivity. Besides being of value for enhancing process efficiency and product quality, the experimental data will be useful for validating process and material models for shear banding in such advanced alloys as well.

Motivations

The use of titanium and its alloys in critical functional applications makes the better understanding of the processes characteristics required to machine them paramount, specifically as it relates to adiabatic shear banding. Ti-6Al-4V is a difficult alloy to machine due to its low thermal conductivity combined with other adverse material properties which leads to adiabatic shear banding-induced force oscillations and increased tool wear through fatigue and impact loading. While there is no easy or direct way to measure these forces, our work is an attempt to provide a quantification of the high frequency forces/accelerations induced due the formation of adiabatic shear bands and hence correlate them with tool, work piece and other process responses.

Objectives

The specific objectives of this project are listed below:

1. To design and assemble piezoelectric and accelerometer-based multi-directional force measurement systems that are capable of capturing the ultra-high frequency force aspects of adiabatic shear banding when machining Ti-6Al-4V alloy,
2. To elucidate the relationships between these ASB-induced machining forces and Ti-6Al-4V chip morphology and process characteristics through a design of experiments of machining runs, and
3. To generate strategies to control ASB-induced process characteristics (by altering process parameters) for improved productivity, surface roughness, and tool wear.

Materials and Methods

The specific workpiece material used in this study is commercially available (grade-5) Ti-6Al-4V. Ti-6Al-4V is a two-phased titanium alloy, comprised of β grains surrounded by equiaxed α grains, leading to an α-β alloy. The cutting tool/insert used in the study is a tungsten carbide-cobalt (WC-Co) turning insert from *Seco Tools* (Model No. CFIR10004D-L4.002.75; tool cutting edge angle of 90°; cutting width of 4 mm), which is recommended for machining titanium alloys. The machining process parameters used in this study were within the lower range of recommended cutting conditions for machining Ti-6Al-4V. Machining experiments were conducted on an instrumented Tormach 15L Slant Pro CNC lathe. The major force/acceleration sensors and data-acquisition (DAQ) devices used in this study were a Kistler miniature Piezo-Beam accelerometer, a Kistler ceramic shear accelerometer, and a dual mode

amplifier combined with a Kistler Piezotron coupler and Kistler piezoelectric quartz dynamometer. The methodology involved the following:

1. First, a commercial piezoelectric force dynamometer will be calibrated, setup, and trail machining tests done to evaluate its capability to reliably measure the ultra-high frequency machining forces generated due to the adiabatic shear banding process during the Ti-6Al-4V chip generation process. Concurrently, an accelerometer-based force measurement system will be designed and setup, that is (already known) to be able to capture ultra-high frequency data. For this, I will first train on the safe and effective use of a CNC lathe along with other research group members. Next, I will be trained on using, acquiring and interpreting the data obtained using a NI-Compact-DAQ hardware using the LabVIEW and MATLAB software.
2. Next, ASB-related data on the two high-frequency machining force components (cutting force and feed force) will be extracted from the raw data obtained from the data acquisition (DAQ) equipment. Relationships will be derived between these ASB-related machining forces and Ti-6Al-4V chip morphology, work piece surface characteristics and tool deterioration. These will involve metallographic preparation of the chips, optical and scanning electron microscopy and spectroscopy and non-contact white light interferometry.
3. Finally, machining experiments will be conducted at untested points in the feed-speed/other-parameter design space to validate a strategy to control ASB characteristics (by altering process parameters), and hence achieve improvement in machining productivity (lower cycle time).assembling and calibrating the force-acceleration measurement sensors and DAQ, conducting a systematic design of experiments of Ti-

6Al-4V machining runs, analyzing the chip morphology and in-process force/acceleration measurements, and finally proposing strategies to alter the input process parameters to control ASB-induced adverse workpiece/tool/process outputs.

Expected Outcomes

The expected outcomes of this research include:

1. A more thorough understanding of the ASB-induced machining forces/accelerations in Ti-6Al-4V machining, and its effects on the workpiece, tool and process from a productivity standpoint.
2. The fabrication and calibration of a coupled piezoelectric and accelerometer-based force-acceleration measurement system that is capable of recording ultra-high resolution/frequency forces/accelerations induced by ASB formations,
3. Correlations between high frequency forces/accelerations and adiabatic shear banding and other chip morphology and process characteristics, and
4. Strategies to improve productivity through the control of ASB-induced workpiece, tool and process characteristics (eventually achieved via process parameter control).

CHAPTER II

BACKGROUND & LITERATURE REVIEW

Force-Sensing Systems Relevant to the Project

Dynamometers

A dynamometer is a load measurement device which can be used to measure multi-directional cutting forces in machining operations.[10] The measurement of cutting force is based on three basic principles: the measurement of elastic deflection of a body subjected to the cutting force, the measurement of elastic deformation (*i.e.*, strain induced by the force), and the measurement of pressure developed in a medium by the force.[10] Depending on the application, one of two general types of dynamometers are used.

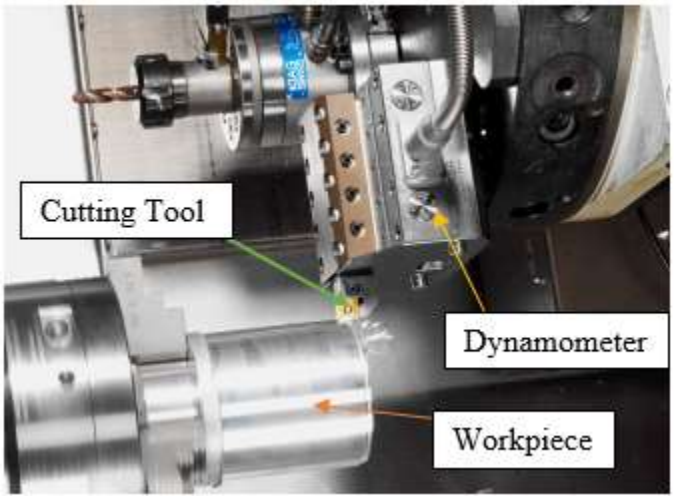

Figure 1: Basic turning operation using a stationary dynamometer where the stationary cutting tool is mounted on the dynamometer

Stationary dynamometers (Fig. 1) are mainly set up on the table or other supporting structure of the machine tool, while rotating dynamometers are connected to the spindle and rotate along with it.[11]

Considering stationary dynamometers, the work piece is often fastened to the dynamometer, and hence the reaction forces in processes (typically drilling or milling) are measured directly. Stationary dynamometers can also be used for turning applications by mounting the stationary cutting tool onto the dynamometer instead of the rotation workpiece (Fig. 1), such as the setup used for this project. The tool is placed on the dynamometer with a suitable tool adapter. Depending on the internal structure of the stationary dynamometer, the forces are measured by one or more multi-directional force sensors and are available at the standard output connector of the dynamometer in the form of charge signals.[10,11]

Rotating dynamometers (RCD) are directly mounted to the machine tool spindle via an adapter interface. The RCD is used mainly in milling and drilling processes. In contrast to stationary dynamometers, only dedicated-component sensors are typically installed in each rotating dynamometer, commonly a torque and/or axial-direction force sensor. In addition to the sensor, the rotor also contains the charge amplifiers (the electronic circuit that converts the charge into voltage and the related telemetry electronics). The measurement data is forwarded to the stationary part of the measuring chain via near-field telemetry, where it is subsequently made available as analog voltage signals.[11] Dynamometers typically have an upper frequency limit around 20 kHz, meaning that force variations higher than that cannot be measured using a dynamometer.

Accelerometers

An accelerometer is a piezoelectric-based device capable of measuring the rate of change of forces (accelerations) as compared to a dynamometer. Accelerometers have commonly used in many industries, such as automotive, navigation, earthquake prediction, robot control systems,

health monitoring of machine tools and other areas that require determination of spatial vibration characteristics such as mobile/communication and gaming systems. A six-axis accelerometer can simultaneously measure of six spatial degrees of freedom (three translational and three rotational) of accelerations.[12]

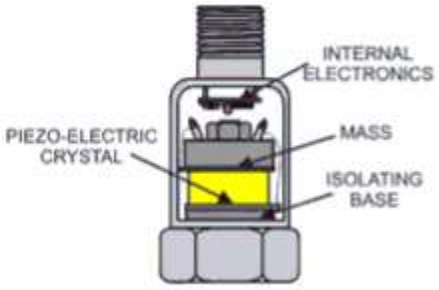

Figure 2: An Isolated Compression Accelerometer: Mass applied to the piezo-electric crystal produces a small electrical charge that is then conveyed to the internal electronics.

The most popular accelerometers are silicon based MEMS (Micro-Electro-Mechanical Systems) accelerometers[13] and piezoelectric accelerometers which make use of a piezoelectric crystal (Fig. 2). Piezoelectric crystals are either man-made or occur naturally. These crystals produce an electrical charge output when compressed, flexed or subjected to shear forces. In a piezoelectric accelerometer a known mass is attached to a piezoelectric crystal which is in turn mounted to the case of the accelerometer. When the body of the accelerometer is subjected to vibration, the mass mounted on the crystal wants to stay still in space due to inertia, and hence compresses and/or stretches the piezo electric crystal. This force causes a charge to be generated in proportion to the acceleration experienced. The charge output is either converted to a low impedance voltage output by the aid of integrated electronics or made available directly as a charge output.[14–16]

Accelerometers are typically capable of higher frequency data acquisition compared to dynamometers. The higher the mounted resonance frequency, the wider the operating frequency range. However, in order to have a higher mounted resonance frequency, it is necessary to have either very 'stiff' piezoelectric elements or less mass (Newton's second law $F = M * A$). The stiffness of the piezoelectric elements is dictated by its material properties, and so a lower mass is generally required for being able to measure ultra-high frequencies. Such a lower mass would however exert less force on the piezoelectric element and the accelerometer would consequently be less sensitive. Therefore accelerometers possessing very high frequency performance are less sensitive; conversely, high sensitivity accelerometers do not have very high frequency measurement capability.[16–18]

Adiabatic Shear Banding in Titanium Alloy Machining

Adiabatic Shear Banding

Adiabatic Shear banding is a high-strain high-rate phenomenon that has been studied extensively because of its importance in the chip generation process of certain alloys which affects the tool, workpiece and process conditions, and specifically for the workhorse titanium alloy, Ti-6Al-4V.[19] An adiabatic shear band is a thin localized area of severe plastic deformation (Fig. 3(a)) and is one of the many material deformation mechanisms that occur in certain metals and metallic alloys that are deformed at a high strain rate prevalent in processes such as metal forming and machining. In titanium alloys, especially Ti-6Al-4V, adiabatic shear banding is primarily caused due its high thermal resistivity and resulting thermal localization[2,3,5]. Though friction from the machining operation also generates heat, this gets dissipated predominantly to the machining tool insert since both the workpiece and the chip have a comparatively lower thermal conductivity.

As metals/metallic-alloys experience an increase in temperature, their resistance to plastic deformation decreases, *i.e.*, the material softens. With any further deformation, a cascading effect results: as more plastic deformation is experienced by the metallic alloy, more heat is generated/experienced, making it easier for the metallic alloy to further deform. This could result in a catastrophic effect which can lead to failure of the structure itself, or be beneficial in one sense in a process such as machining for easier chip flow, but affect it adversely as well by promoting high-temperature initiated tool wear.[5,19,20]

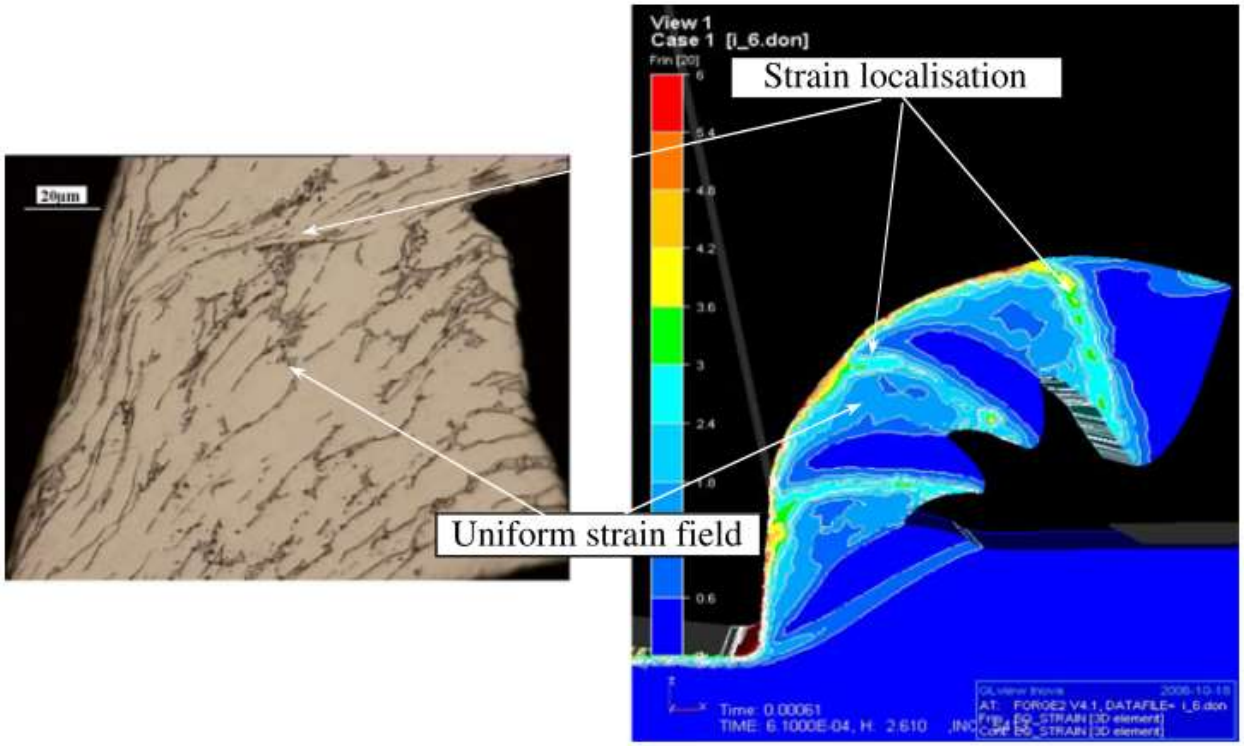

Figure 3: Strain Localization vs Uniform Strain Field [28] *Experimental (Left) and simulated (Right) chips obtained with a cutting speed of 60 m/min and a feed of 0.1 mm. A finite-element simulation result of a dry turning operation showing the strain contour plot on the chip having regions of high strain localization, indicating Adiabatic Shear Banding.*

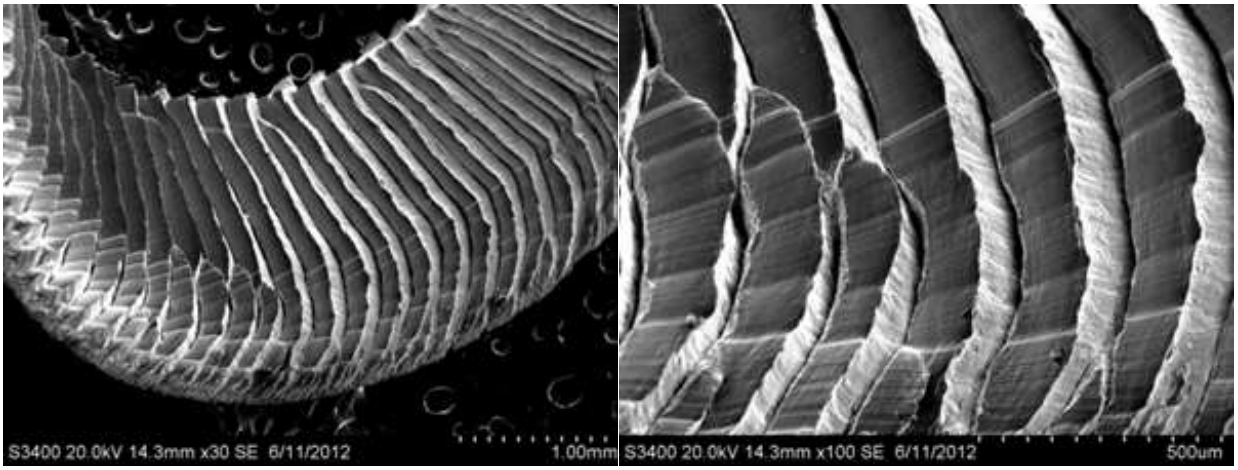

Figure 4: High resolution scanning electron microscope image of Ti-6Al-4V turned chip surface showing the high degree of segmentation.

In the context of machining, the chip is a process waste. Nevertheless, its study allows for a detailed physical understanding of the cutting process (and its optimization).[19] In titanium alloys, especially Ti-6Al-4V, the chip formation process is often characterized by cyclic localization of plastic deformation which is the result of adiabatic shear forces that create a very characteristic "saw-tooth" or segmented chip pattern.[1,3,5–7,19] Each "saw-tooth" is bounded by two shear planes characterizing the saw teeth periodicity.[19] This chip segmentation causes a variation of the chip's section. Consequently, this change will have a considerable influence on the variation of cutting forces and chip evacuation speed as well.[5,19–21]

Specific aspects of the chip morphology are interesting from a scientific and engineering point of view because it is formed dynamically during the machining operation and directly affects the tool, workpiece and process as a whole. In order to elucidate the interactions of the tool material/geometry with the workpiece material being machined, it is essential to understand how this segmented chip is formed (Fig. 4), and how it is affected by ASB characteristics (Fig. 5).[19] It potentially can help predict/determine not only the tool and workpiece surface responses,

but indirectly also the potential resulting structural loads and the power required to remove a given volume of metal at a certain rate.

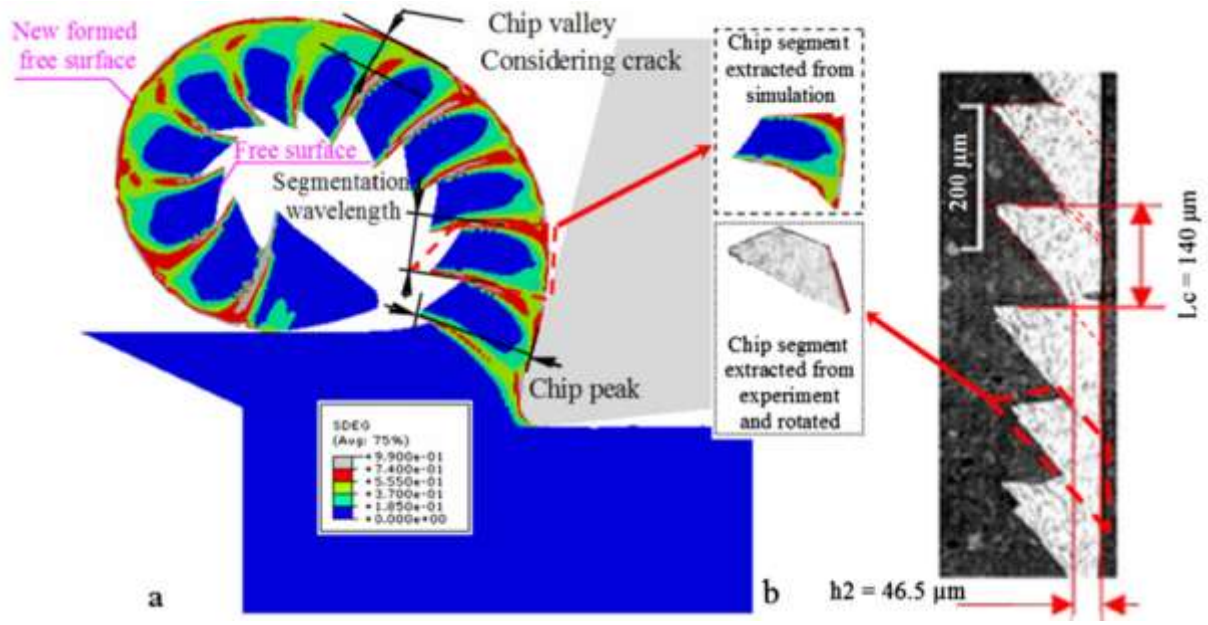

Figure 5: (a) Chip formation mechanism simulation, (b) 2D profile of Ti-6Al-4V chip containing shear bands [19]

Implications for the Tool and Workpiece

As previously stated, the low thermal conductivity of titanium alloys especially influences tool wear, and particularly those wear mechanisms initiated by high temperatures such as dissolution and diffusion wear. The thermal softening of the tool material as well as the higher diffusion rates enabled by the high temperatures encountered cause tools used for machining Ti-6Al-4V to often fail prematurely and unexpectedly. Additionally, the ASB formation induces a high frequency oscillatory force component profile onto the tool as well leading to failure due to fatigue and impact; as as result Ti-6Al-4V has been classified as a 'difficult-to-machine' material. When considering the workpiece-side of the interface, *i.e.*, at these localized zones of high thermal energy (ASBs), the material is weakened thus lowering the stiffness at the localization. Now, with a lower Young's modulus and high shear strength, work hardening will

occur if chips do not meet a minimum thickness due to the fact that the tool will plastically deform, compress, and harden the titanium work piece[1,2,4]. The minimum chip thickness is a requirement based on the size effect which states that the depth of cut and the chip load must be greater than the tool tip radius in order to form a chip. If not, when machining, the tool will encounter and need to remove the now work-hardened material. This then leads to high flank wear in the tool[4,22,23]. Further, the ASB and other chip morphology parameters have a direct influence on the workpiece surface roughness, surface/sub-surface residual stress states and damage as well.

CHAPTER III

MATERIALS & METHODS

Experimental Setup

Setup of Equipment and Sensors

For the experiments in this project, a Tormach SlantPro 15L CNC lathe was used, the main specifications of which are given in Table 1. A coated tungsten carbide-cobalt grooving tool was used to perform the cuts on the Ti-6Al-4V tube. The width of the cutting tool (4 mm) used was greater than the thickness of the workpiece being cut so that forces induced were only along two axes (Fig. 6). Also shown below in Fig. 7 is the general connection diagram, and in Fig. 8 a setup of the equipment and sensors including the dynamometer and the accelerometer.

Table 1: Tormach 15L Slant Pro Lathe Specifications

Mechanical		
Travels	X-axis	10"
	Z-axis	12"
Feed Rates	Rapid Speeds	60 IPM
Key Dimensions	Table Length	26"
	Table Width	6"
	Tool Holding	Gang tooling plate with three T-slots 0.625" (5/8") Center Slot: 0.00 + 0.004" – Outer Slots: 0.000 + 0.008"
		Manual quick change tool post.
		8-position turret
	Swing Over Bed	15"
	Swing Over Carriage	6.2" (turret or manual tool post); 1.88" (gang plate)
	Footprint	55" W x 66" H x 29" D
Spindle	Speed Range	300-3500 RPM (5C), 175-2500 RPM (6"chuck)
	Horsepower	3 hp continuous
	Drive System	Cartridge style spindle with double V-belt transmission
	Design	D1-4 spindle w/ removable 5C taper insert

Figure 6: The tool insert used had a width greater than the width of the workpiece, therefore only two forces were induced. Thrust and cutting forces are present, as feed direction and depth of cut direction are the same.

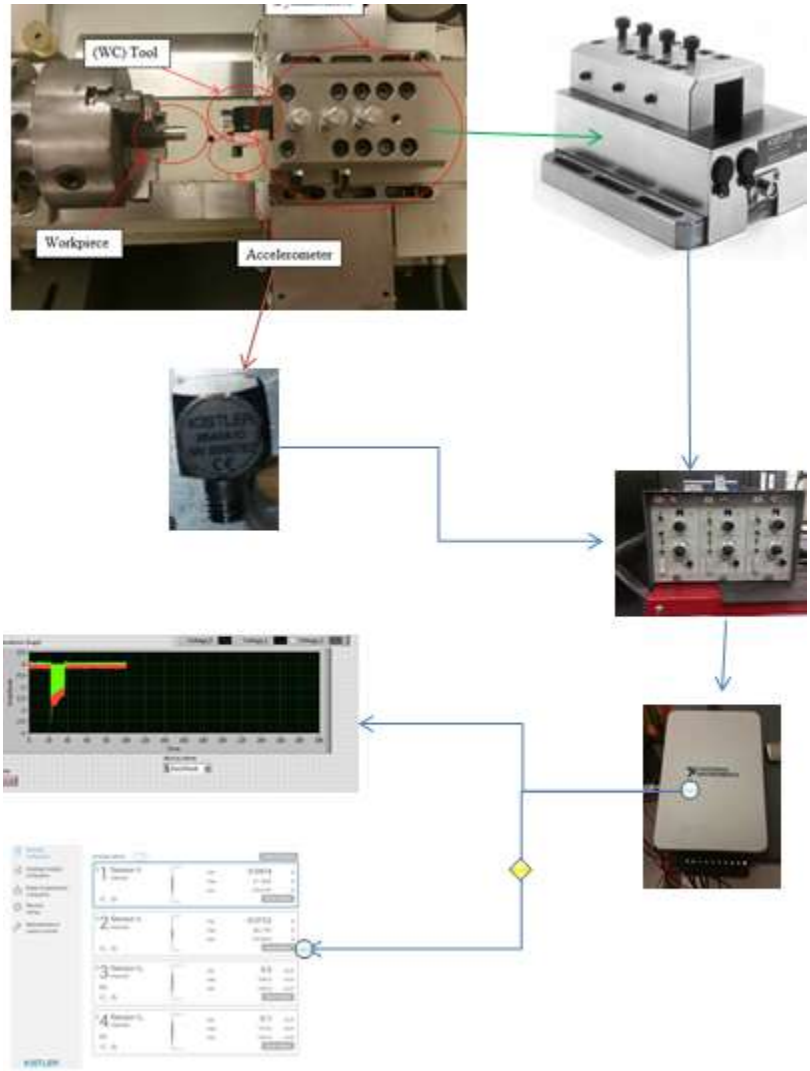

Figure 7: The complete connection diagram. Individual components and their functions are described below

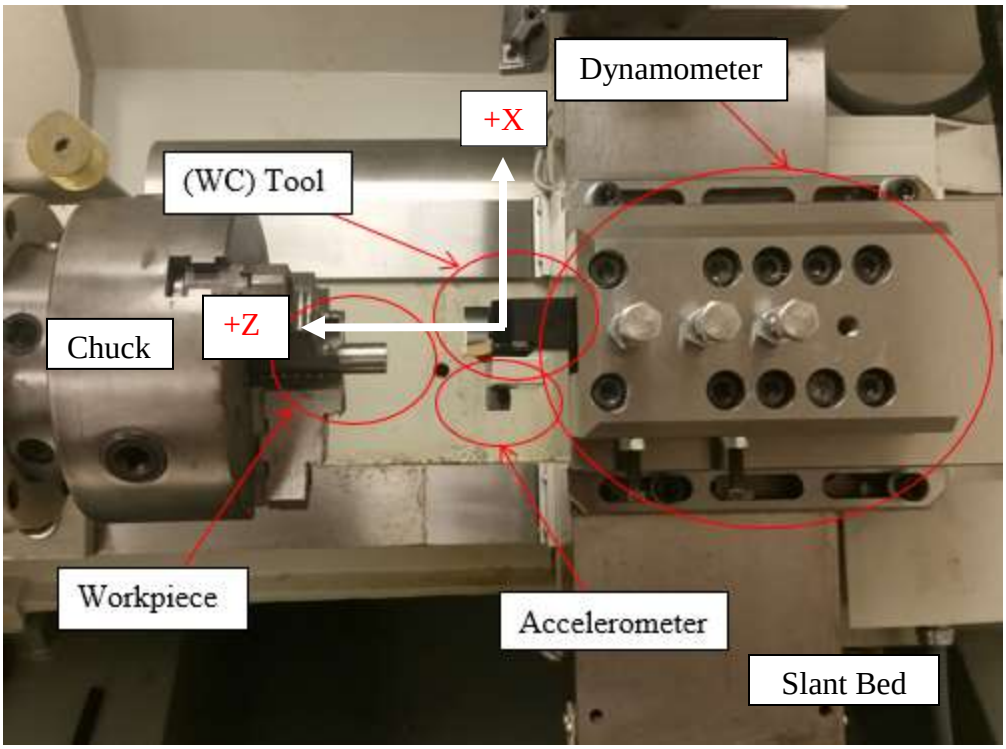

Figure 8: General setup of the sensors and hardware for measuring multi-directional forces and accelerations when turning Ti-6Al-4V using a carbide tool

The dynamometer used was a Kistler 9265B force plate combined with a Kistler 9441B tool holder (Fig. 9); its schematic is given in Fig. 10, and specifications in Table 2. The accelerometer was a Kistler type 8694M1 as shown in Fig. 11, and specifications in Table 3.

Figure 9: Kistler Dynamometer used in this project: Type 9265B – 9441B[11]

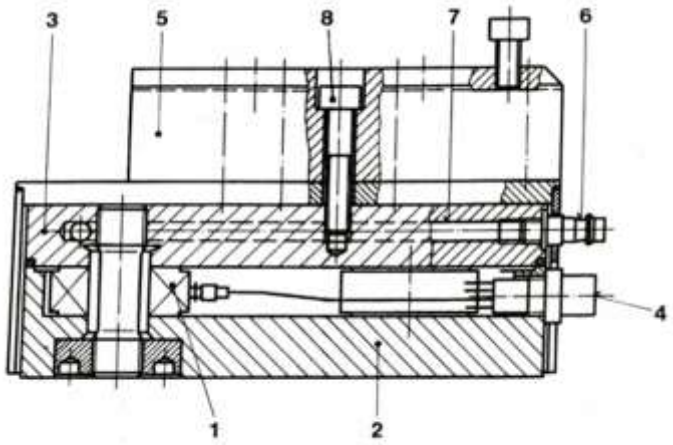

Basic unit with toolholder Type 9441B

1	Force sensor
2	Base plate
3	Top plate
4	Connecting plug
5	Working adapter (Toolholder)
6	Cooling agent connection
7	Cooling system
8	Mounting screws for working adapter

Figure 10: Dynamometer Schematic

Table 2: Kistler Dynamometer Specifications

Technical Data			
Type			**9265B + 9411B**
Range	F_x, F_y	kN	–15 ... 15[2]
	F_z	kN	0 ... 30[2]
Calibrated partial range	F_x, F_y	kN	0 ... 1,5
	F_z	kN	0 ... 3
Overload	F_x, F_y	kN	–20/20
	F_z	kN	–12/40
Threshold		N	<0,01
Sensitivity	F_x, F_y	pC/N	≈–8
	F_z	pC/N	≈–3,7
Linearity, all ranges		%FSO	≤±0,5
Hysteresis, all ranges		%FSO	≤0,5
Cross talk		%	≤±2
Rigidity	c_x, c_y	kN/µm	≈0,8
	c_z	kN/µm	≈2
Natural frequency	f_n(x, y)	kHz	≈1,5
(mounted on flanges)	f_n(z)	kHz	≈2,5
Operating temp. range		°C	0 ... 70

Figure 11: The accelerometer measures changes in velocity, and converts them into an electrical signal for the DAQ to read

Table 3: Accelerometer Specifications[24]

Specification	Unit	Type 8694M1
Acceleration range	g	±500
Acceleration limit	gpk	±1000
Threshold, nom. (noise 100 µVrms)	grms	0.025
Sensitivity, ±5 %	mV/g	4
Resonant frequency mounted, nom.	kHz	80
Frequency response, ±5 %	Hz	10 … 20000
Amplitude non-linearity	%FSO	±1
Time constant, nom.	s	0.5
Transverse sensitivity nom.	%	<5

Setup of Data Acquisition System

The Data Acquisition System (DAQ) used consisted of a Kistler Miniature Piezo Beam Accelerometer, a Kistler Ceramic Shear Accelerometer, a Model 5004 Dual mode Amplifier, combined with and a Kistler Dynamometer. The output from the dynamometer and accelerometer is an electrical current that then is fed into the signal amplifier (Fig. 12, Fig. 13), which in turn is fed into Data Acquisition System (Fig. 14; specs in Table 4) that is subsequently run in a LabVIEW VI (Fig. 15, Fig. 16) or a Kistler interface (Fig. 17). The resulting data is then graphed via a Matlab code (see Appendix) to convert the electrical signals to force values.

Figure 12: The signal amplifier takes the small voltages given off by the dynamometer, amplifies them, and then feeds them into the DAQ

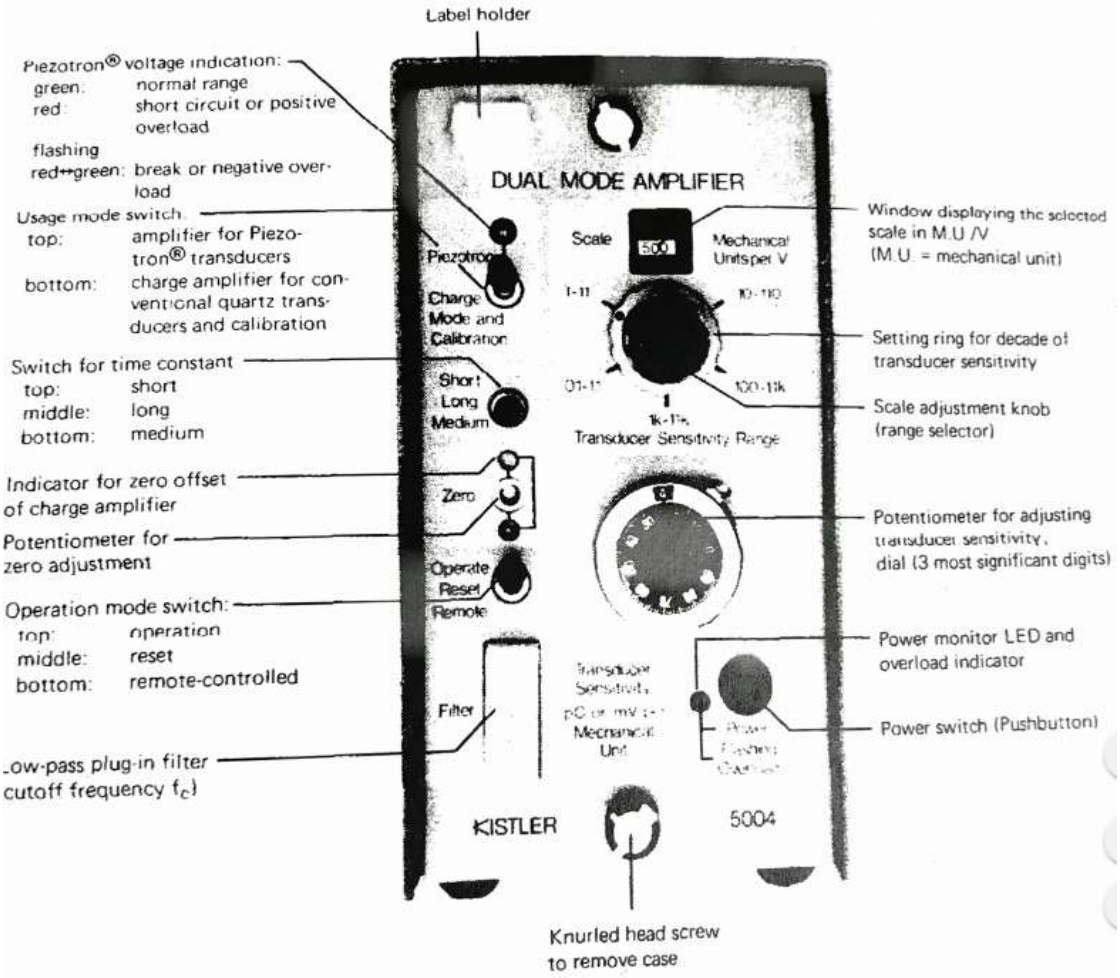

Figure 13: Amplifier Diagram

Figure 14: National Instruments Data Acquisition System: takes voltage signals from the signal amplifier and sends them to a LabVIEW program for processing. The model used was a NI-9215 DAQ coupled with a cDAQ-9171 Chassis.

Table 4: NI -9215 DAQ Specification[25]

Stability	
Offset drift	60 µV/°C
Gain drift	10 ppm/°C
CMRR (at 60 Hz)	–73 dB min
Input bandwidth (–3 dB)	420 kHz min
Input impedance	
Resistance	
With screw terminal	1 GΩ
With BNC (between any two AI– terminals)	200 kΩ
Capacitance	25 pF
Input bias current	10 nA
Input noise	
RMS	1.2 LSB_{rms}
Peak-to-peak	7 LSB
Crosstalk	–80 dB

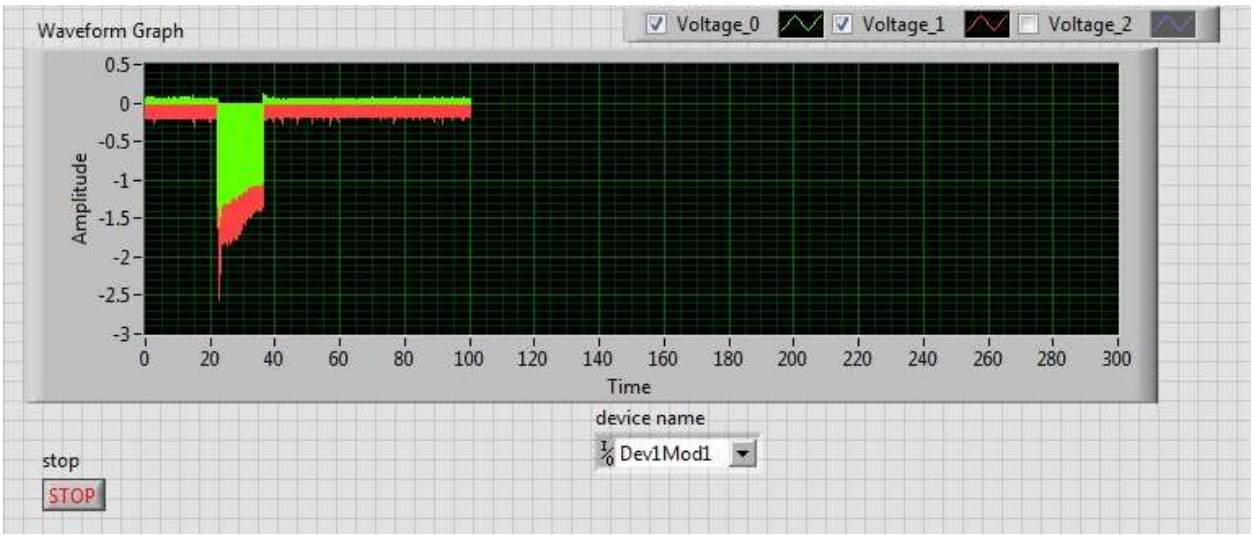

Figure 15: LabVIEW VI: takes signal from DAQ and outputs raw numerical data.

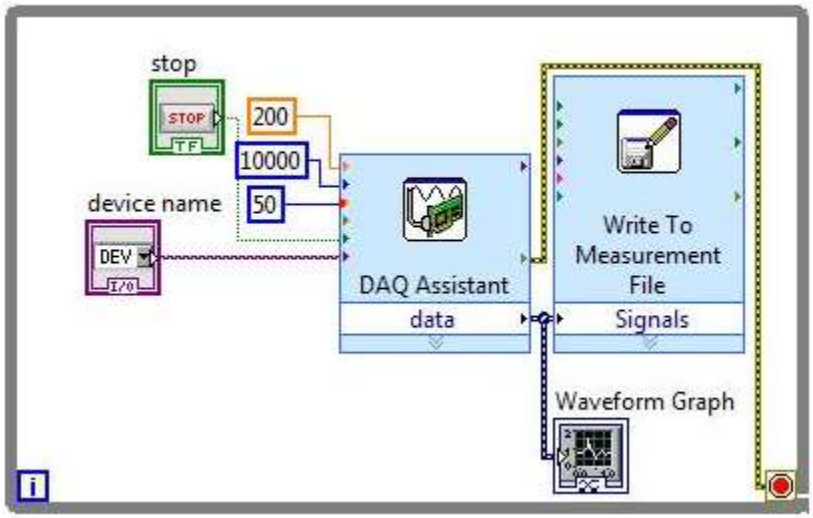

Figure 16: LabVIEW VI circuit diagram, showing the virtual layout of the program

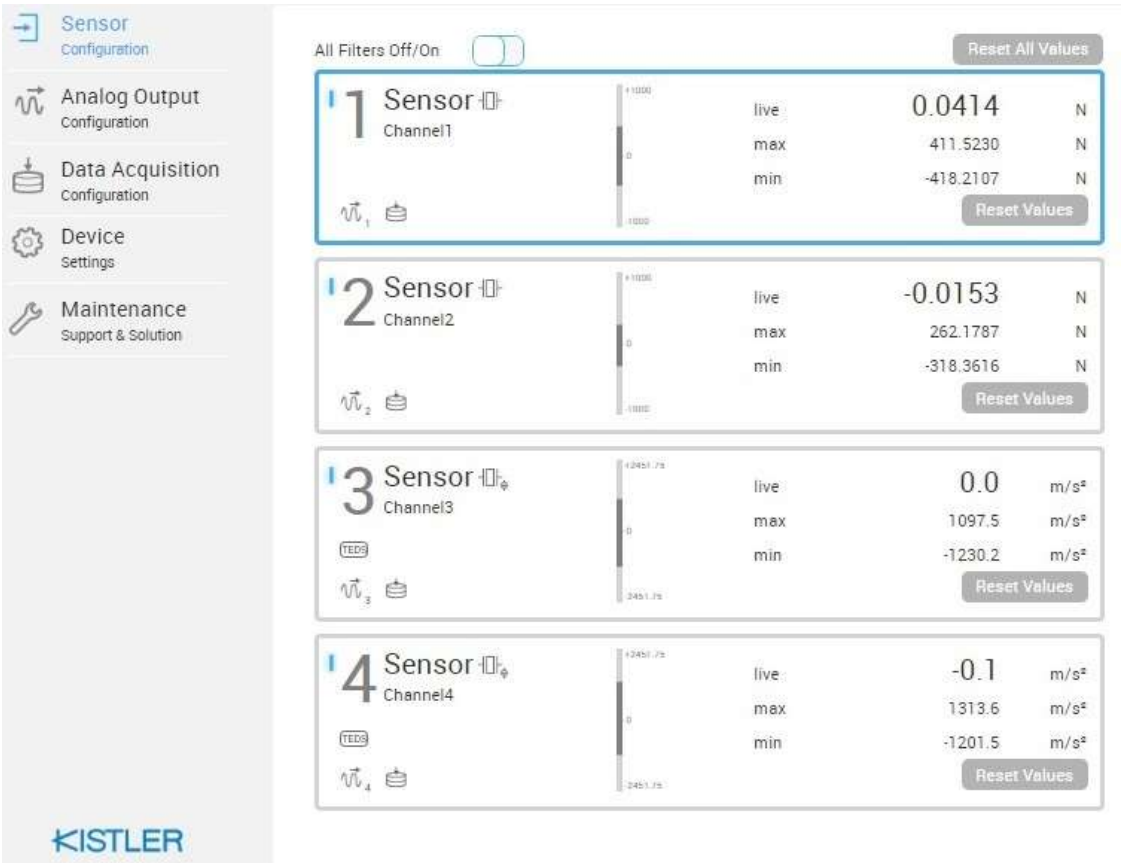

Figure 17: Kistler Lab amplifier interface: takes voltages from the accelerometer and dynamometer and outputs that data to be run through a MATLAB code. Sensors 1 and 2 are the thrust force and cutting force respectively, while sensors 3 and 4 are the thrust acceleration and cutting acceleration respectively

Tools & Materials

The workpiece material used in this study was commercially available grade-5 titanium alloy. The workpiece specimen (Fig. 18) was a Ti6Al-4V tube: outer diameter .645” and inner diameter 0.484”. The relevant physical and thermal properties of Ti-6Al-4V are shown below (Table 5). The cutting tool (Fig. 19) used was a tungsten carbide-cobalt grooving tool.

Figure 18: Ti-6Al-4V Tube OD = 0.645", ID = 0.0484"

Table 5: Ti-6Al-4V Physical & Thermal Properties

Property	**Metric**	**English**
Density	4.43 g/cc	0.16 ib/in^3
Hardness (Brinell)	334	334
Ultimate Tensile Strength	950 MPa	138000 psi
Yield Tensile Strength	880 MPa	128000 psi
Modulus of Elasticity	113.8 GPa	16500 psi
Shear Modulus	44 GPa	6380 psi
Shear Strength	550 GPa	79800 psi
Thermal Conductivity	6.7 W/m-K	46.5 BTU-in/hr-ft^2-˚F
Melting Point	1604 – 1660 ˚C	2920 – 3020 ˚F

Figure 19: Coated Tungsten Carbide-Cobalt Grooving Tool

Calibration

Calibration of equipment is essential for accurate understanding and analyses of the data. Calibration was done (Fig. 20) by measuring the voltage output of the dynamometer while using an already calibrated load cell (Fig. 21; specifications are given in Table 6) to establish a base line to compare the voltage output to. Different ranges/levels of forces were applied and held for about 5-second each while the responses from the dynamometer (Fig. 23) and load cell (Fig. 22) were recorded. A load to voltage relationship (Fig. 24) was then used to relate output voltages to loads. Calibration was done both in the cutting and thrust directions using the dynamometer.

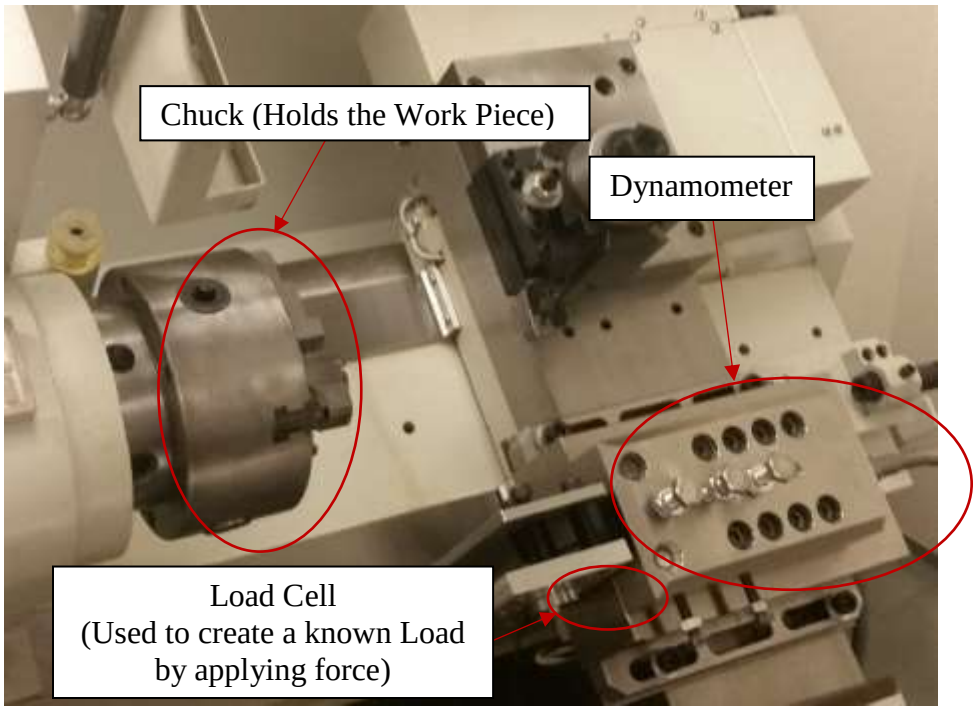

Figure 20: Calibration Setup, including Load cell, and Dynamometer

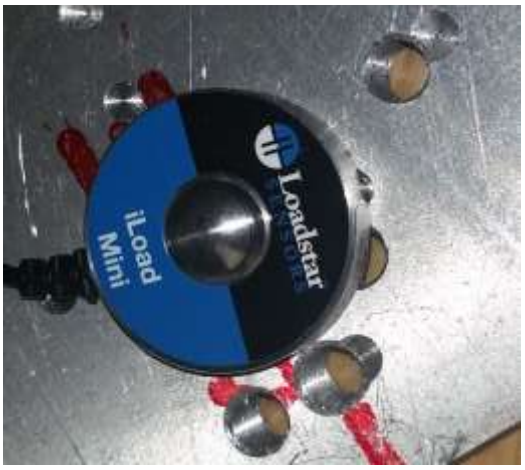

Figure 21: Loadstar iLoad Mini load cell used in calibration. (See specifications below)

Table 6:Load Cell Specification[26]

Load Cell Specifications

Accuracy w/tare (% of FS)	Non-linearity	Hysteresis	Non-repeatability
10, 50, 100, 200 lb.	±1 %	±1 %	±1 %
Response Rate	10 Hz		
Mechanical			
Safe Overload	to 150% of capacity		
Deflection	0.002-in at capacity typical		
Sensor Size	1.25 OD, for height see table above		
Electrical			
Input Power	Regulated 5V at 60 mA		
Output	5V TTL variable frequency signal when Control = 1, Frequency Output = F_{sensor} when Control = 0, Frequency Output = F_{ref} $F_{comp} = F_{sensor} - K * F_{ref}$ Compensation factor K provided by Loadstar		
Connections	integrated 6 ft. cable with pigtail for terminal attachment or 5 pin male USB mini-B Connector		
Environmental			
Creep, in 20 min	±0.03 % of full scale		
Operating Temperature Range	10°C to 40°C, non-condensing		
Temperature Effect on Span	up to ±0.05 % full scale/°C (from calibration temperature)		

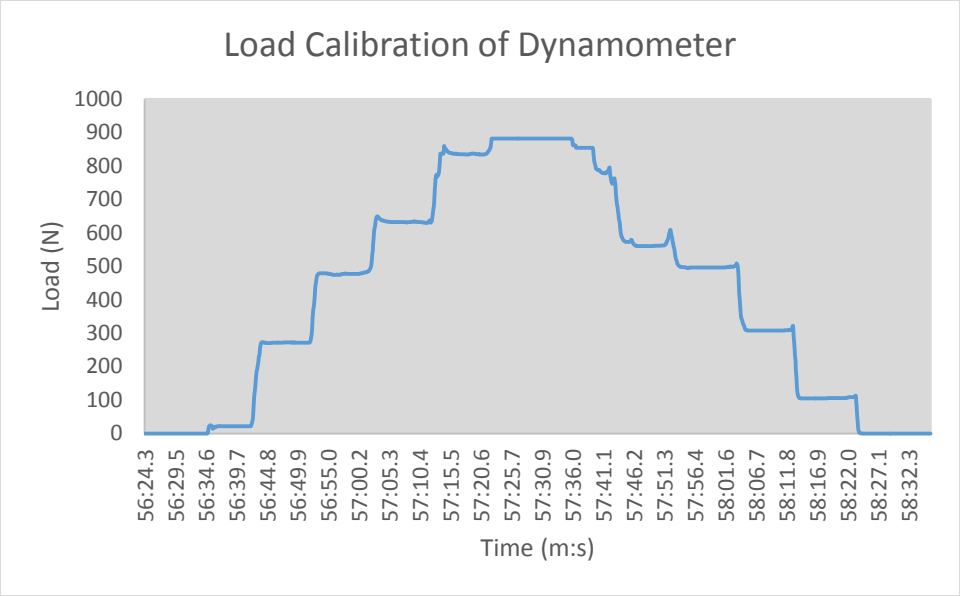

Figure 22: Load calibration of Dynamometer: Load Cell output is shown. Dynamometer was loaded with various known loads the voltage output (below) is then compared to the known loads/ times.

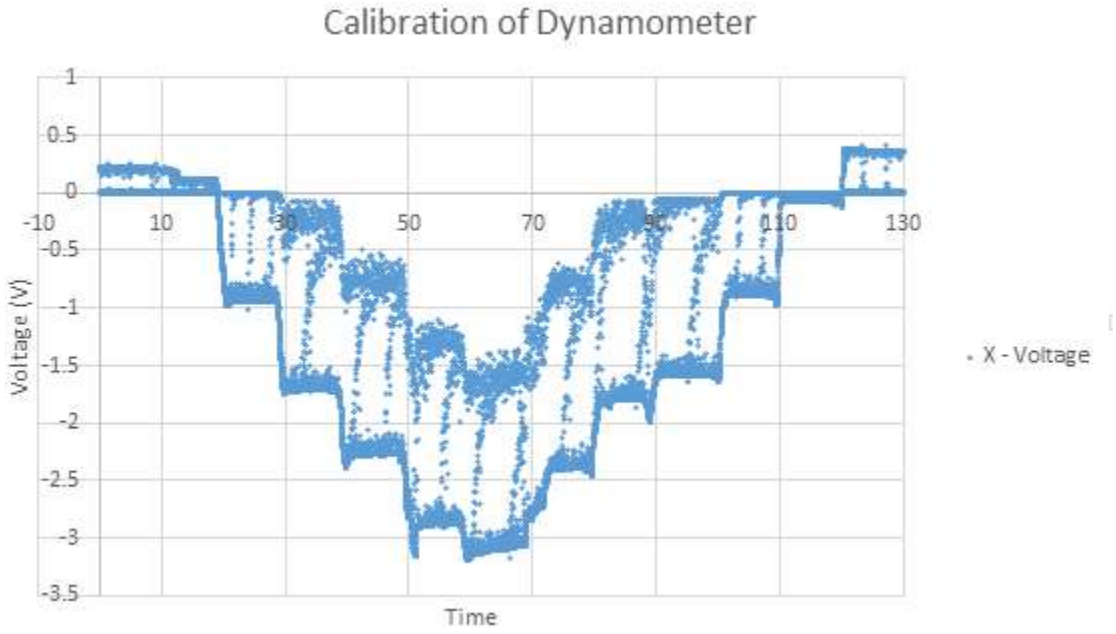

Figure 23: Dynamometer calibration raw voltage data vs. Time

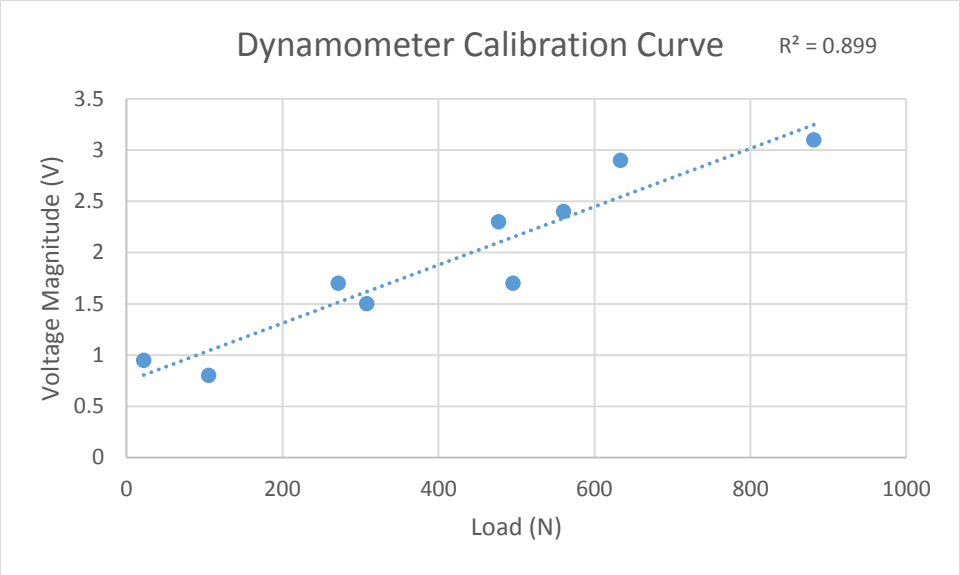

Figure 24: The calibration Curve shows the relationship between voltage given off by the dynamometer, and the applied load

Design of Experiments

Cutting experiments were done (Table 7) with feed rates of 0.01in/rev. and 0.005 in/rev. as well as cutting speeds of 9, 30 and 45 m/min. The number of revolutions per cut was held constant at 20 revolutions to generate a chip length of 35.6 mm in each case. For this, first the prepared specimen was secured in the lathe, and then the necessary CNC code generated and run. While cutting was taking place, accelerometer and dynamometer data was simultaneously being acquired. After the cut, the data and machining chips was saved for later analysis.

Table 7: Table Showing the Design of Experiments done

Run	Feed Rate (in/rev)	Cutting Speed (m/min)	Depth of Cut (µm)	Rotational Speed (rpm)	Length of data (sec)
1	0.01	9	254	199	6.03
2	0.01	30	254	663	1.81
3	0.01	45	254	994	1.21
4	0.005	9	127	199	6.03
5	0.005	30	127	663	1.81
6	0.005	45	127	994	1.21

CHAPTER IV

RESULTS & ANALYSES

Force/Acceleration Results from Experimental Runs

To elucidate the relationships between ASB-induced machining forces, chip morphology and process characteristics, the design of experiments of machining runs (specified earlier in Table 7) was conducted. Each of the following graphs (Fig. 25-52) were produced by running the raw data obtained during cutting experiments from the dynamometer and accelerometer through the MATLAB Code (see Appendix) for generating appropriate plots. The blue lines represent the raw data, while the red lines represent the running averages of the forces and accelerations measured.

Both forces and accelerations in the thrust and cutting directions were measured in each case. In general, average cutting forces varied from 150 - 300N, and average thrust forces from about 200 - 600N. Also, the average accelerations in the cutting direction varied from about 1 - 11g, while acceleration in the thrust direction varied from about 1 - 6g.

Run 1: f = 0.01 in/rev.; S = 9 m/min.

Run 1: Acceleration Data

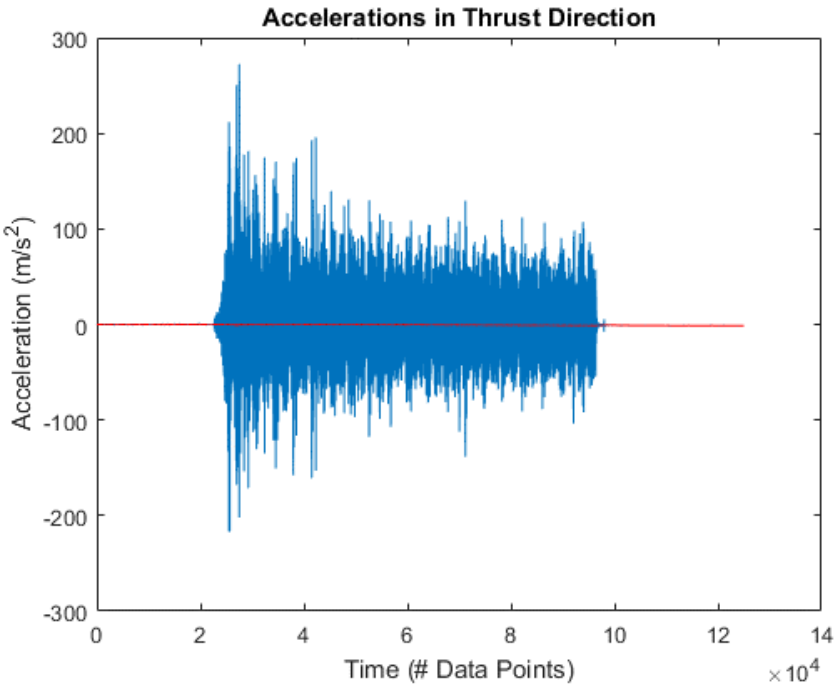

Figure 25: Thrust Direction Acceleration

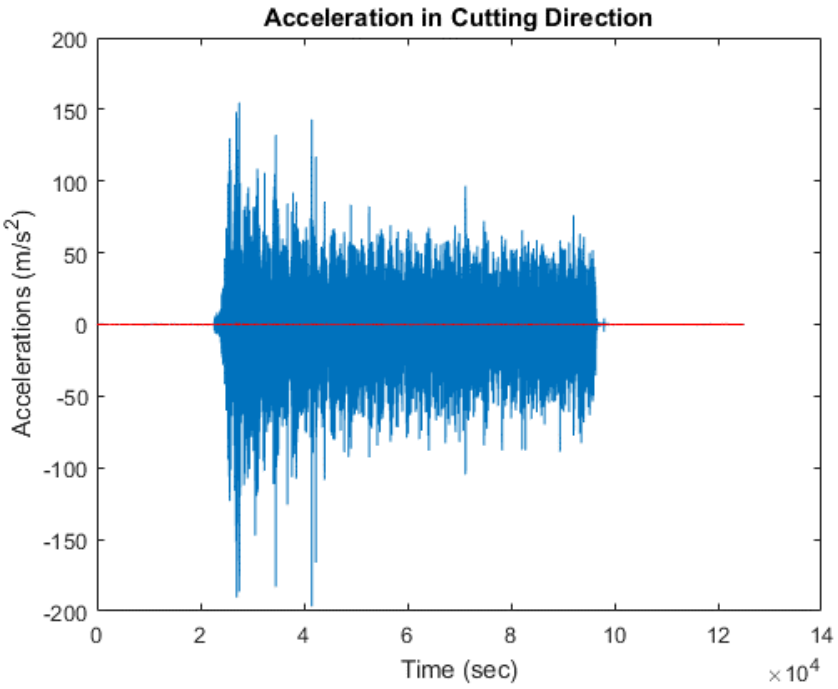

Figure 26: Cutting Direction Acceleration

Run 1: Force Data

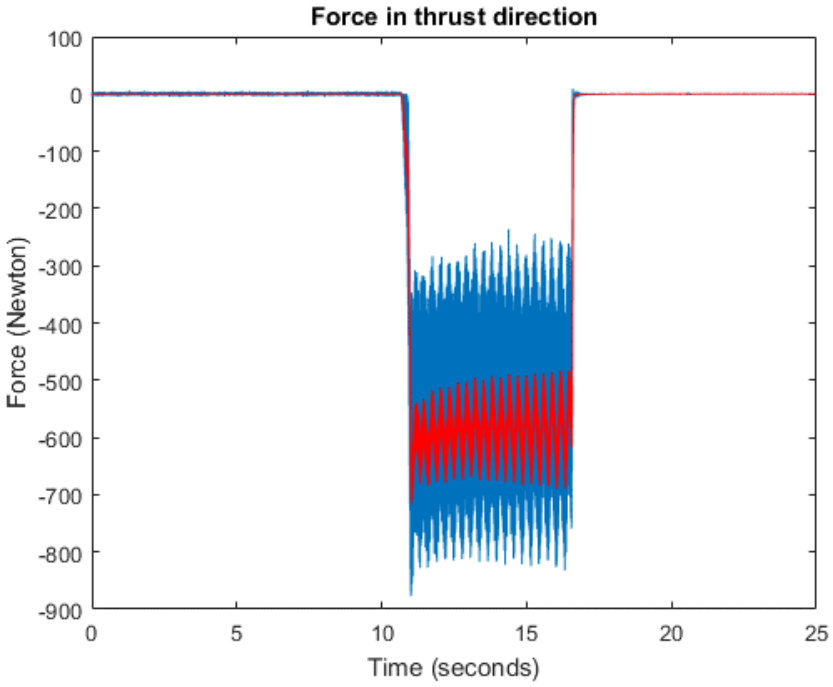

Figure 27: Thrust Force vs. Time

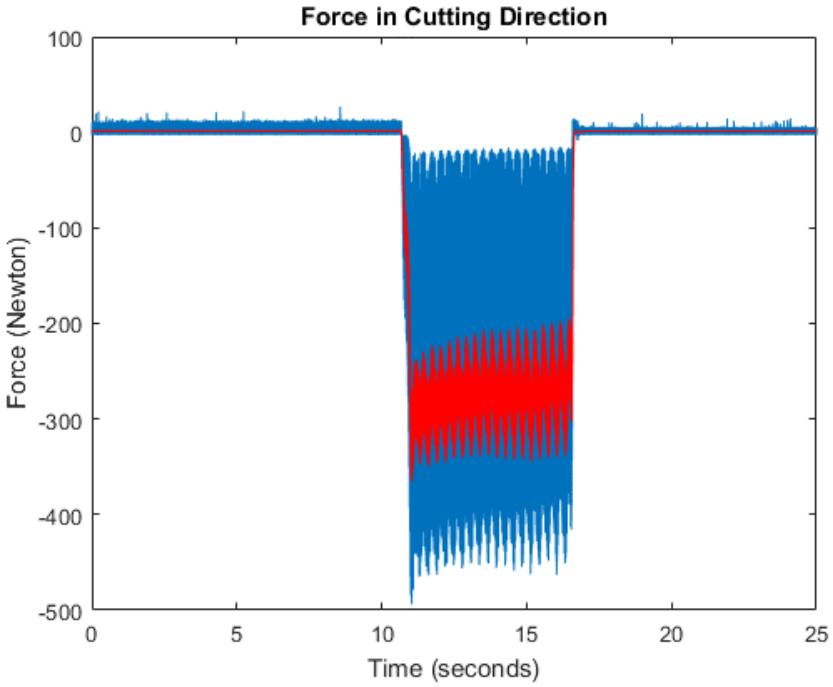

Figure 28: Cutting Force vs. Time

Run 2: f = 0.01 in/rev.; S = 30 m/min.

Run 2: Acceleration Data

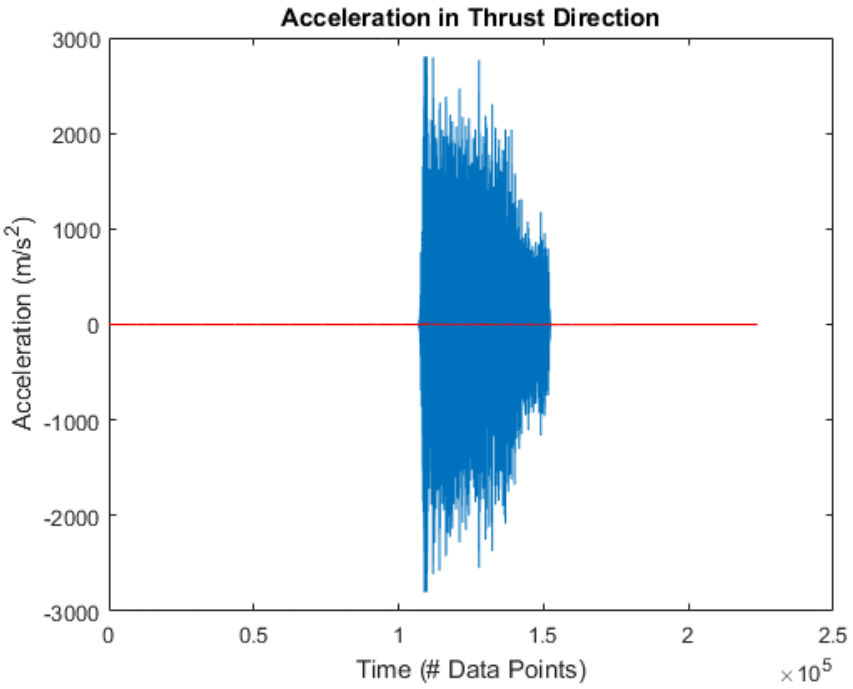

Figure 29: Thrust Direction Acceleration Data

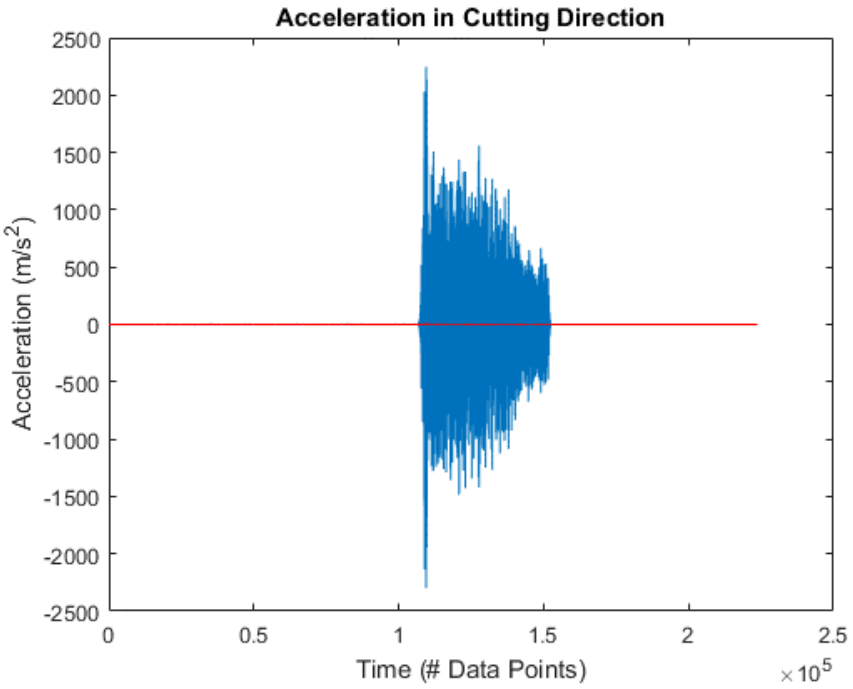

Figure 30: Cutting Direction Acceleration Data

Run 2: Force Data

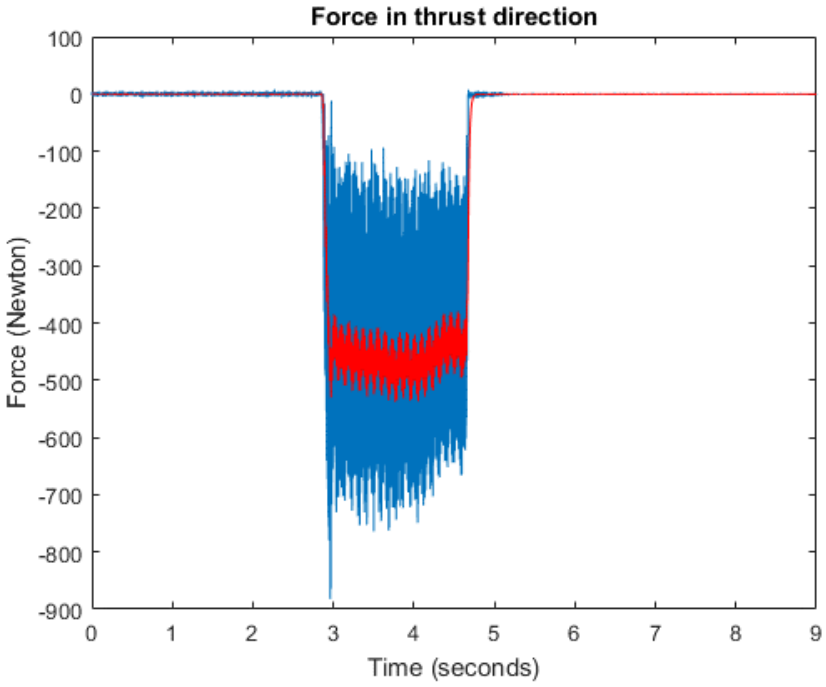

Figure 31: Run 2 Thrust Force Data

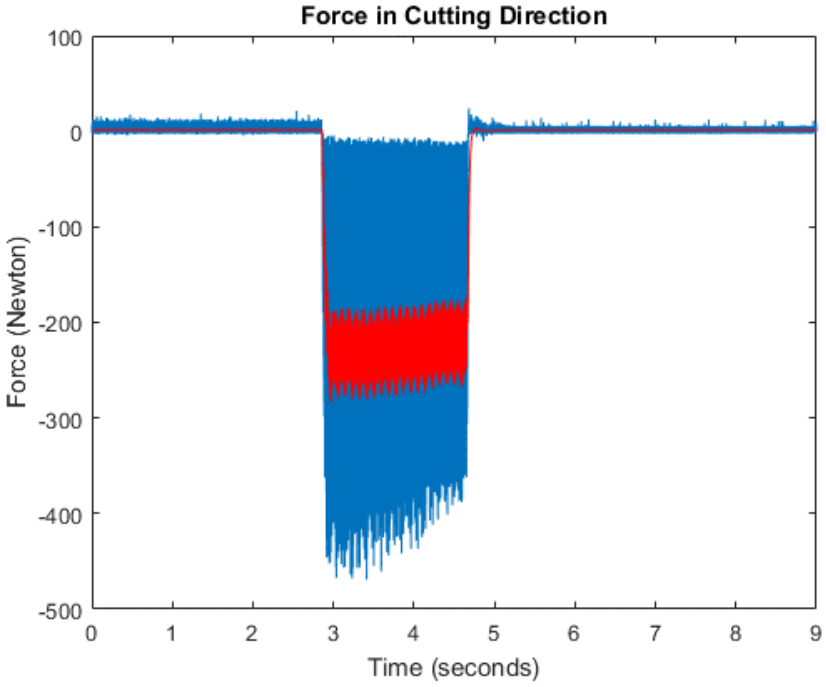

Figure 32: Run 2 Cutting Force Data

Run 3: f = 0.01 in/rev.; S = 45 m/min.

Run 3: Acceleration Data

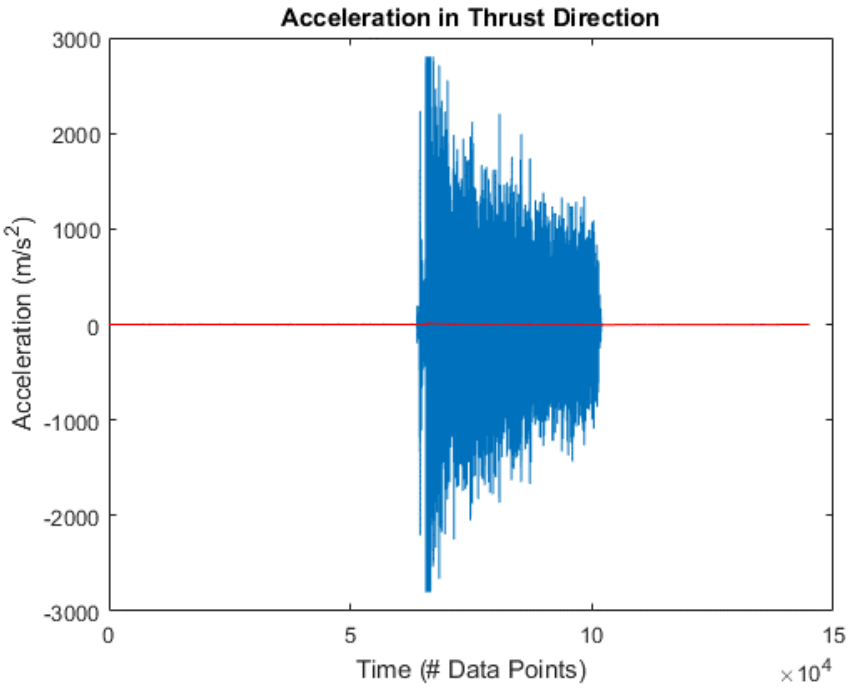

Figure 33: Run 3 Thrust Acceleration Data

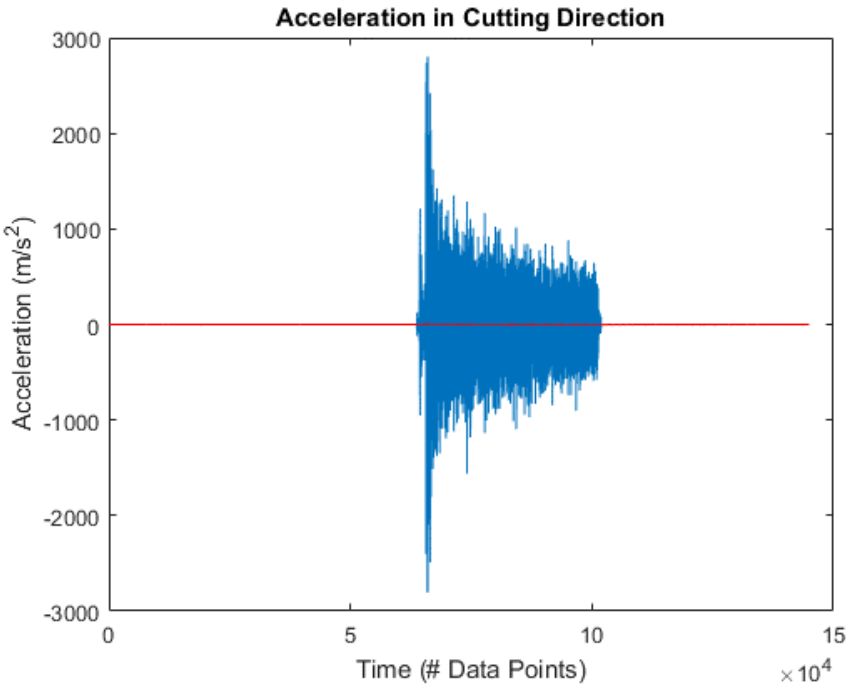

Figure 34: Run 3 Cutting Force Data

Run 3: Force Data

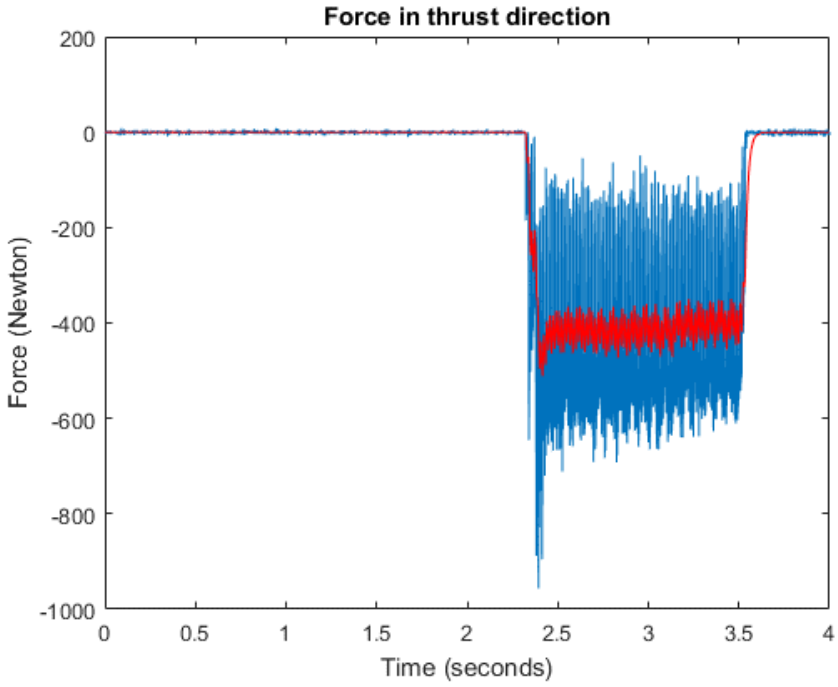

Figure 35: Run 3 Thrust Force Data

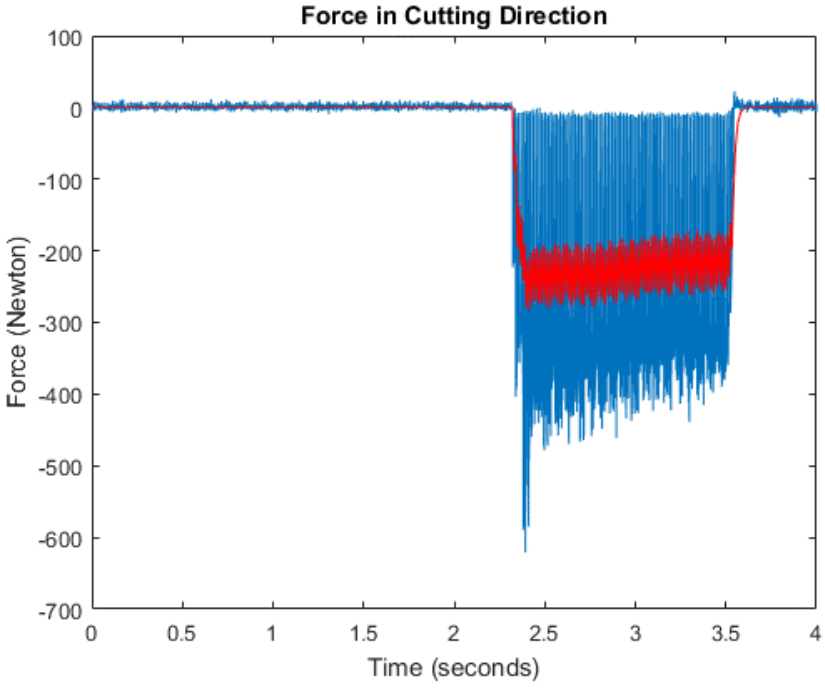

Figure 36: Run 3 Cutting Force Data

Run 4: f = 0.005 in/rev.; S = 9 m/min.

Run 4: Acceleration Data

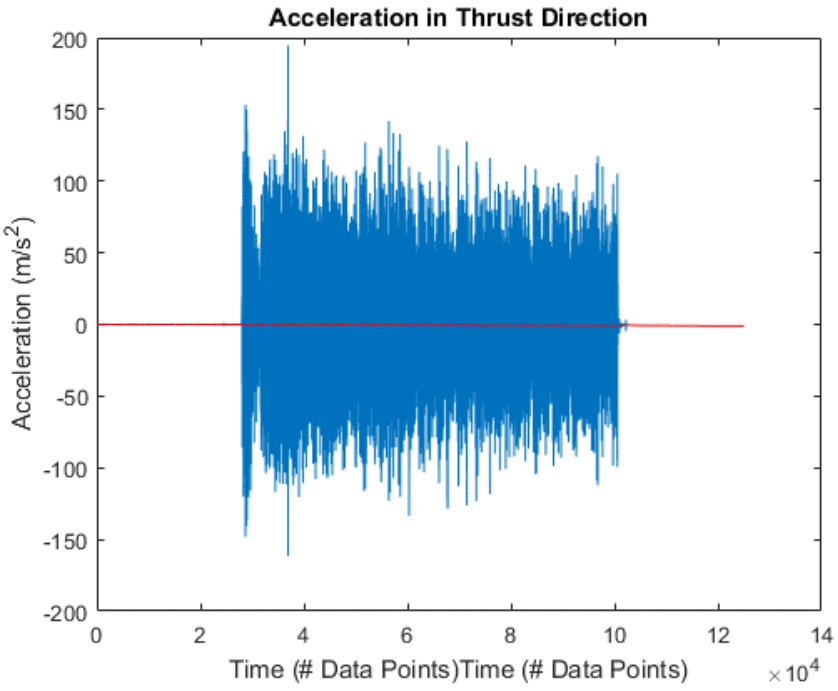

Figure 37: Run 4 Thrust Acceleration Data

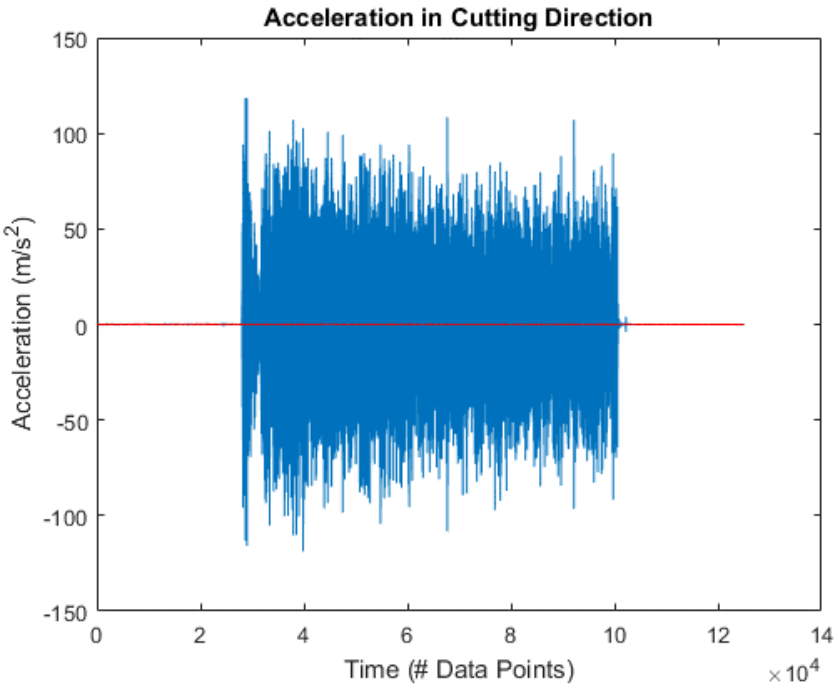

Figure 38: Run 4 Cutting Acceleration Data

Run 4: Force Data

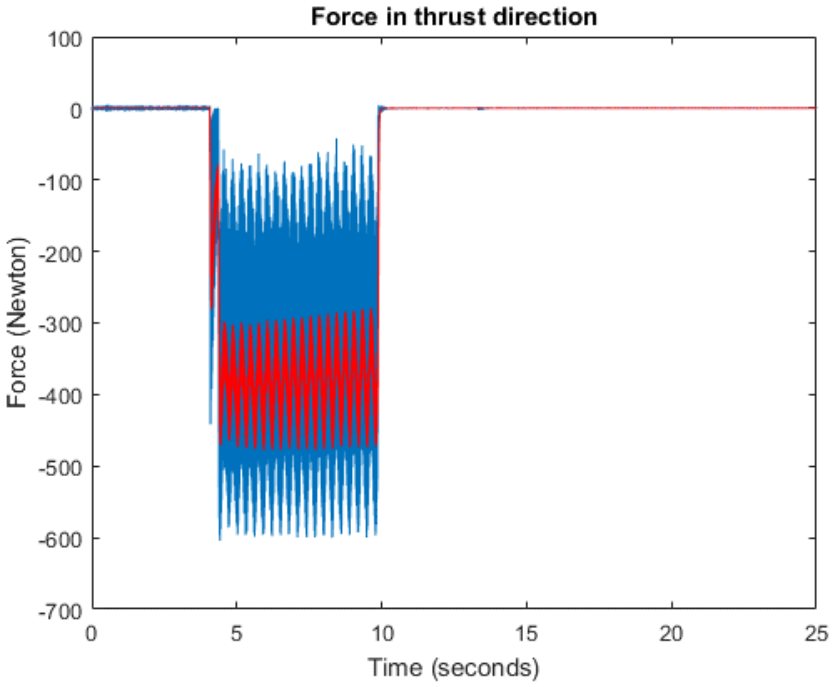

Figure 39: Run 4 Thrust Force Data

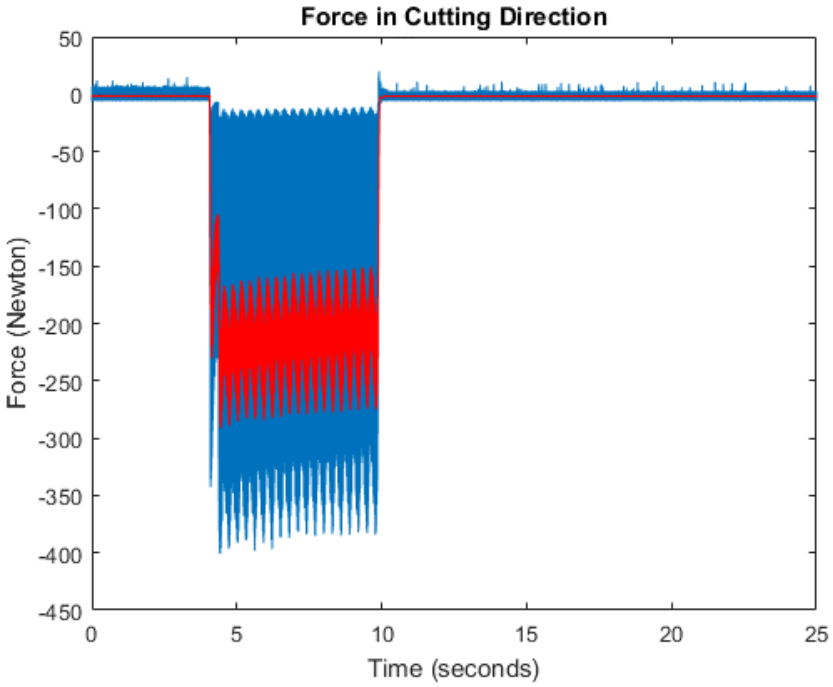

Figure 40: Run 4 Cutting Force Data

Run 5: f = 0.005 in/rev.; S = 30 m/min.

Run 5: Acceleration Data

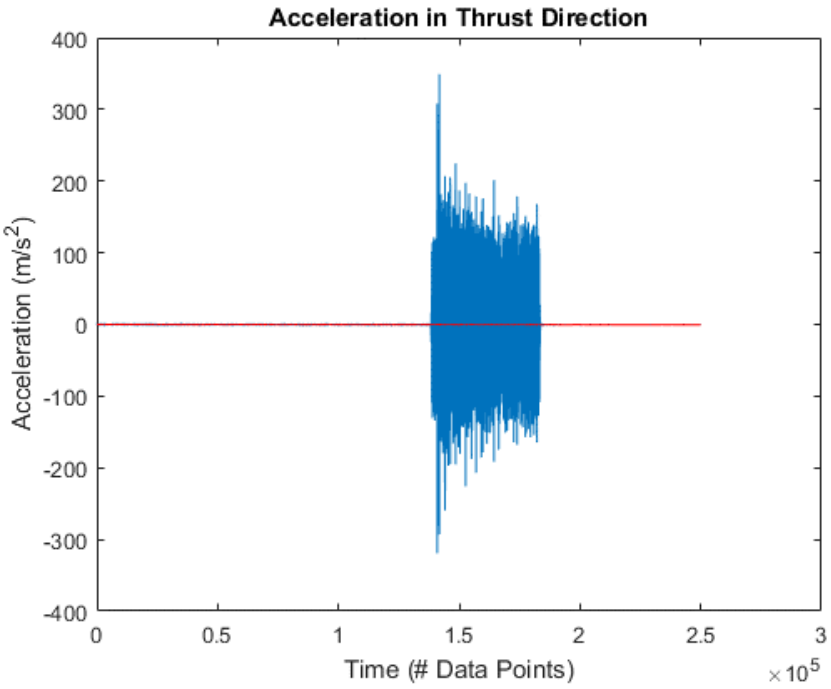

Figure 41: Run 5 Thrust Acceleration Data

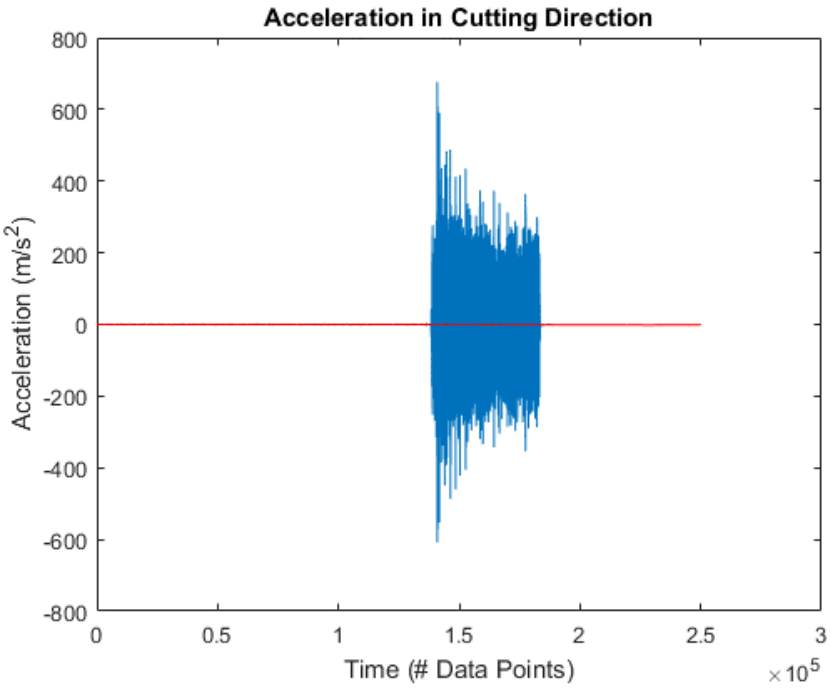

Figure 42: Run 5 Cutting Acceleration Data

Run 5: Force Data

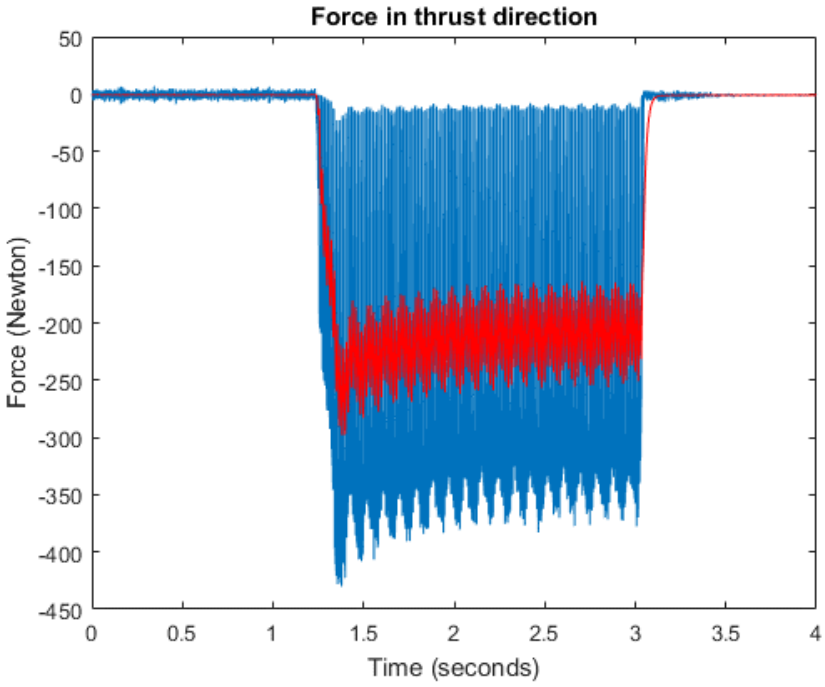

Figure 43: Run 5 Thrust Force Data

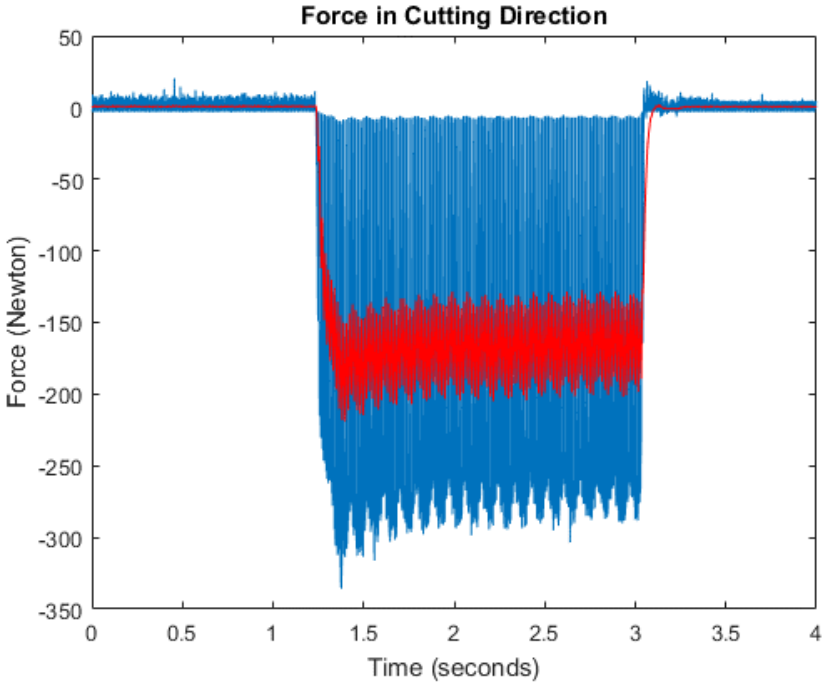

Figure 44: Run 5 Thrust Force Data

Run 6: f = 0.005 in/rev.; S = 45 m/min.

Run 6: Acceleration Data

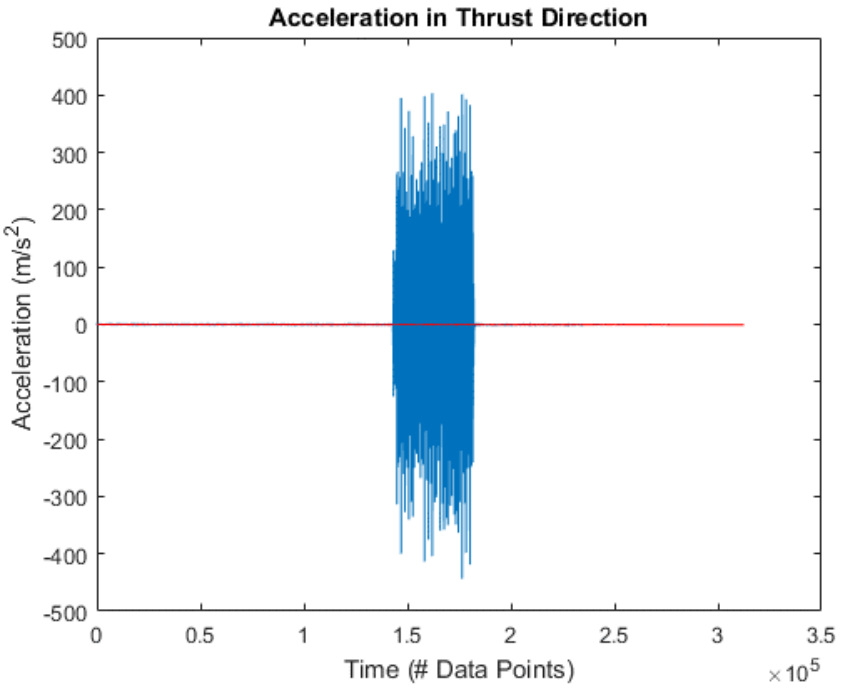

Figure 45: Run 6 Thrust Acceleration Data

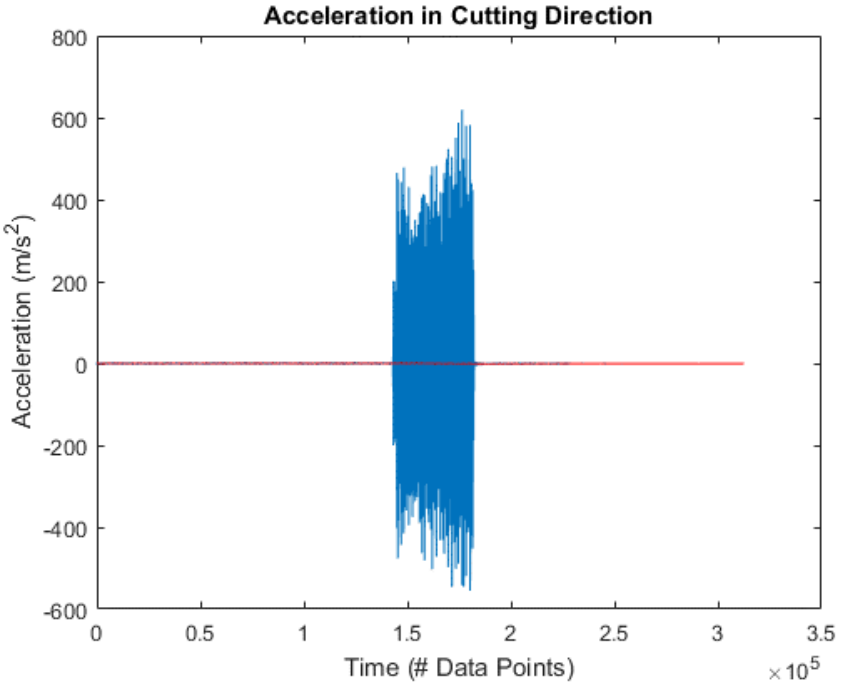

Figure 46: Run 6 Cutting Acceleration Data

Run 6: Force Data

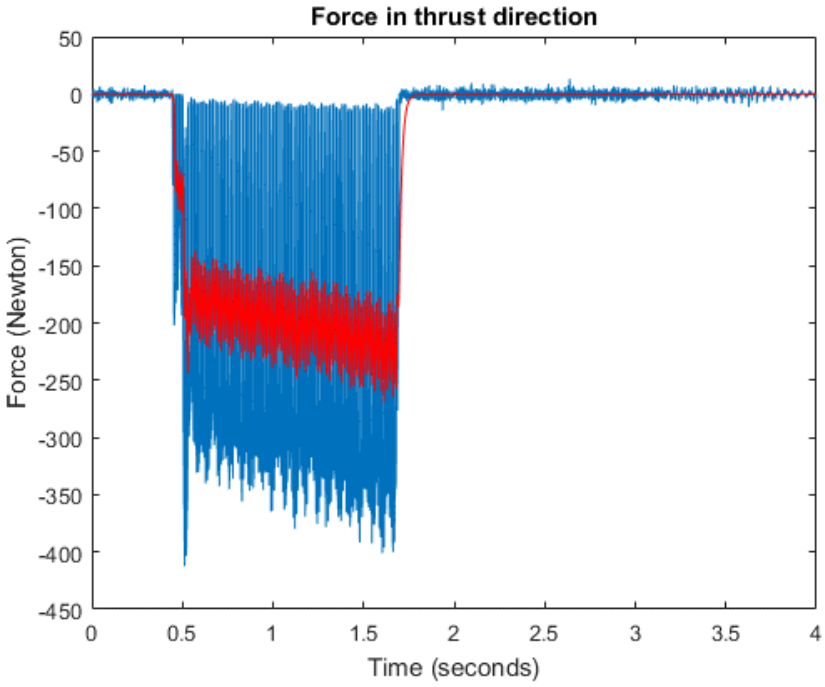

Figure 47: Run 6 Thrust Force Data

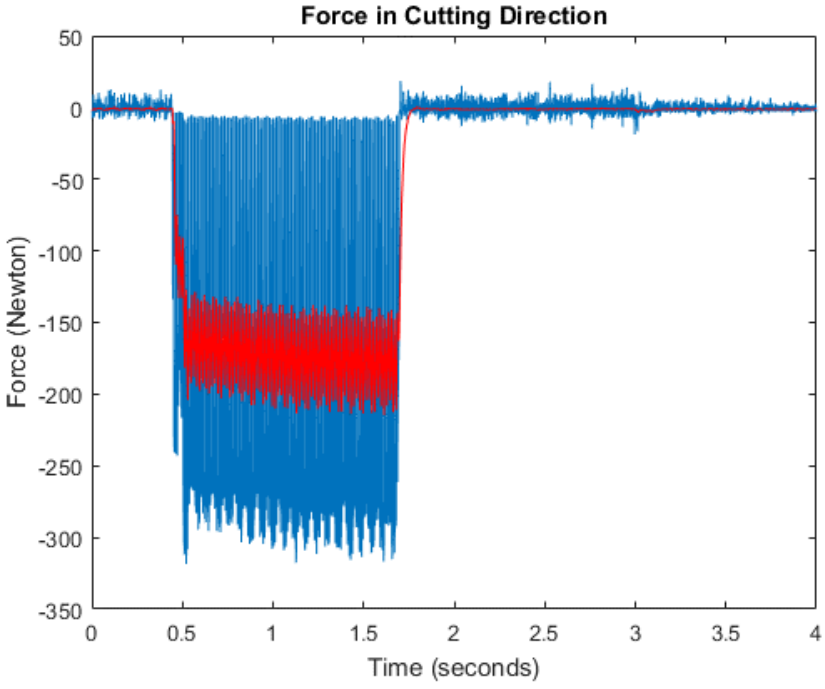

Figure 48: Run 6 Cutting Force Data

Fast Fourier Transforms

Below are the Fast Fourier Transforms for run one. Fourier transforms take a signal as input, then output the dominant frequencies of that signal.

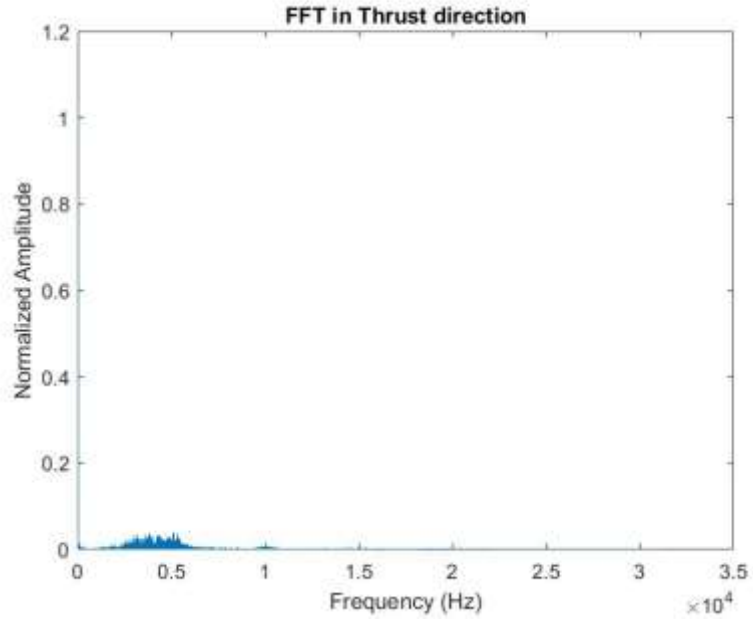

Figure 49: FFT for Run 1 Thrust Acceleration

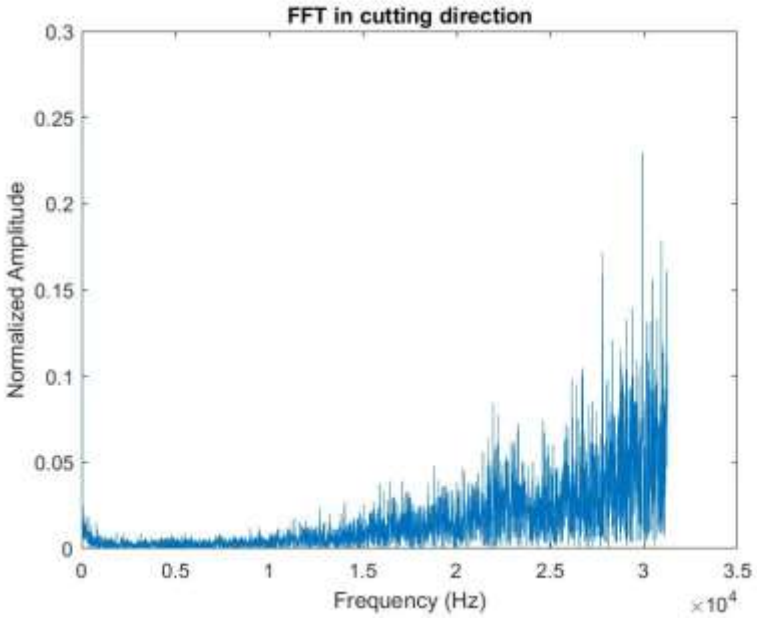

Figure 50: FFT for Run 1 Cutting Acceleration

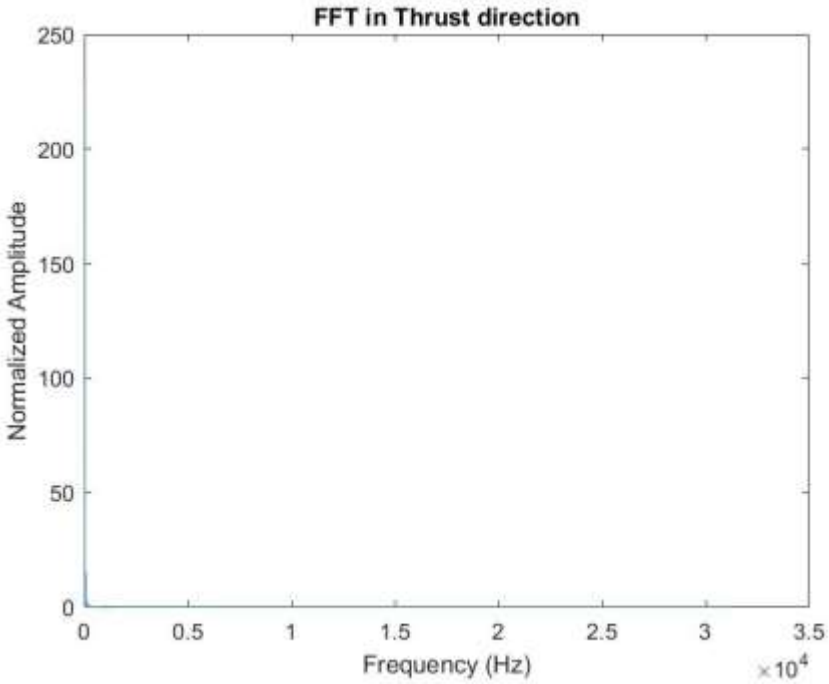

Figure 51: FFT for Run 1 Thrust Force

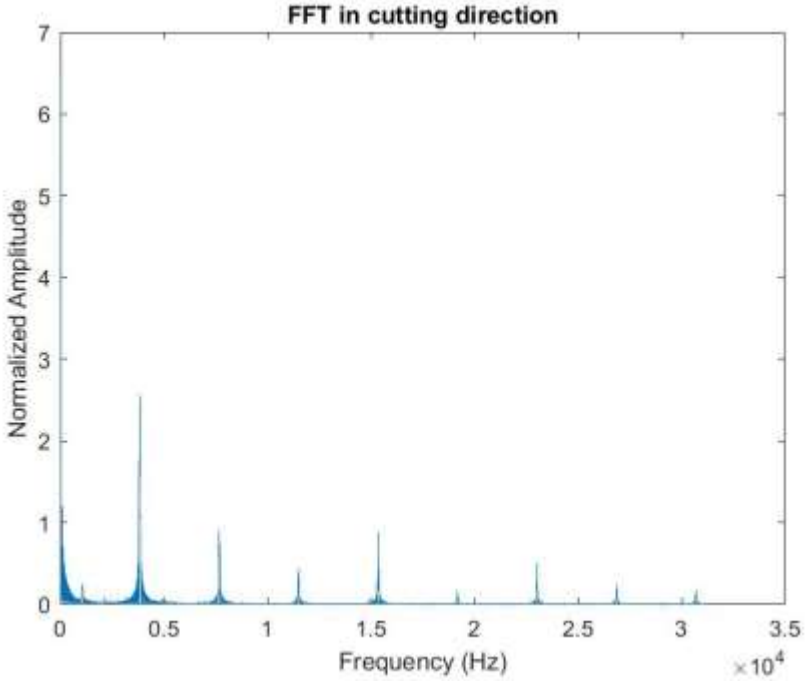

Figure 52: FFT for Run 1 Cutting Force

Relations between Force/Acceleration and process Conditions

Average values for thrust force and cutting force are compiled (Table 8), as well as accelerations in the two directions. These are then compared to process conditions (Fig. 53-56).

Table 8: Force values shown are absolute values as raw data values were negative

Run	Feed	Speed	Average Thrust Force	Average Cutting Force	Average Cutting Acceleration	Average Thrust Acceleration
	(in/ Rev.)	(m/min)	(N)	(N)	(m/s^2)	(m/s^2)
1	0.01	9	581	291	11.8	8.8
2	0.01	30	466	230	91.9	49.8
3	0.01	45	410	226	108.9	61.6
4	0.005	9	384	215	14.2	11.1
5	0.005	30	205	166	14.5	9.5
6	0.005	45	193	171	13.3	7.9

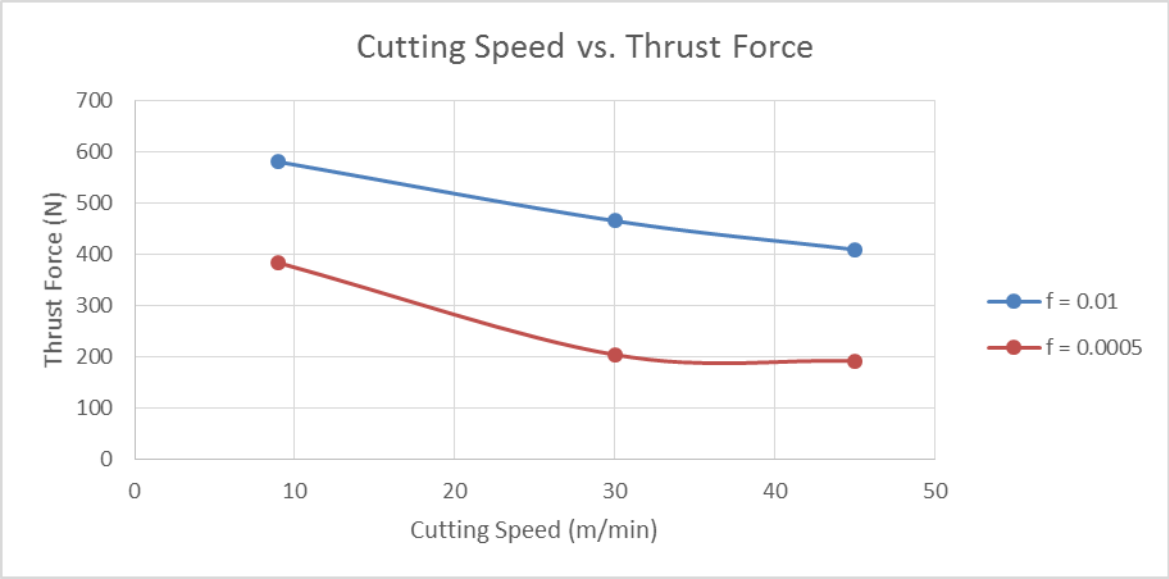

Figure 53: Cutting Speed vs. Average Thrust Force

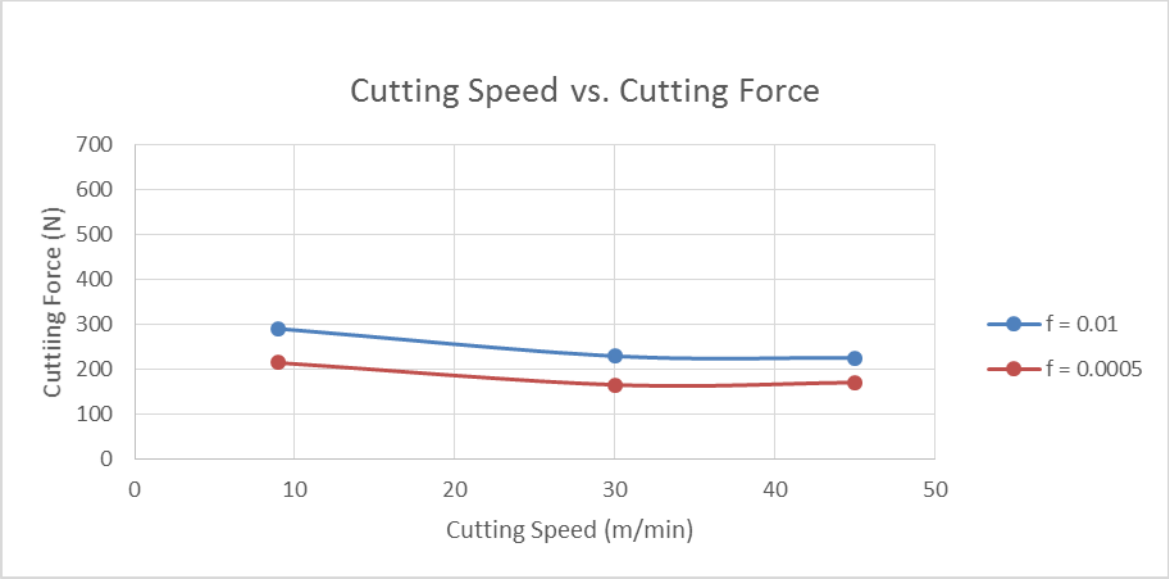

Figure 54: Cutting Speed vs. Average Cutting Force

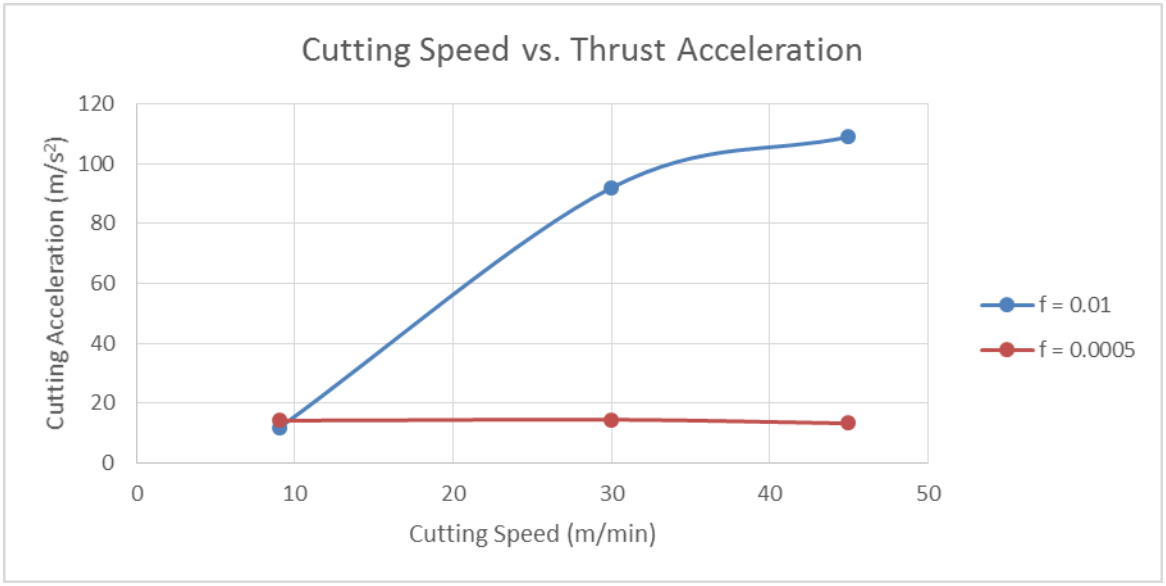

Figure 55: Cutting Speed vs. Thrust Acceleration

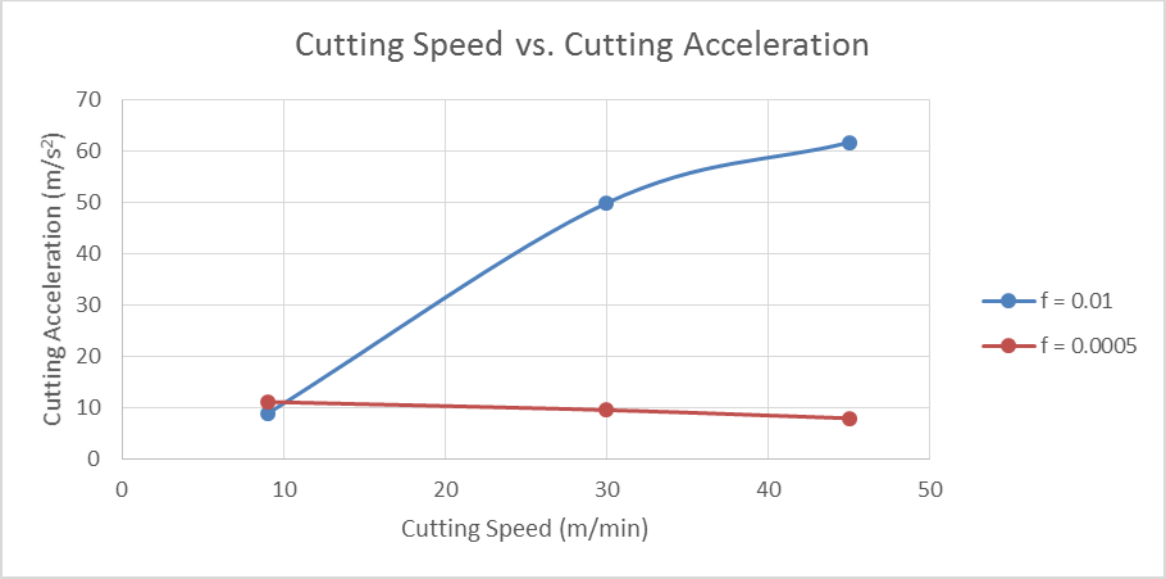

Figure 56: Cutting Speed vs. Cutting Acceleration

Relations between Chip Morphology and Process Conditions

Typically, Ti-6Al-4V turning chips are jagged in appearance, especially at higher speed and depths of cut. The chip morphology parameters are compared with process conditions (Fig. 57-60); the major chip morphology parameters include the following - a_1 is the segment spacing, a_2 is saw-tooth height, a_3 is the continuous portion height, and L_c is shear band spacing as shown (Fig. 57). Measured parameter values are compiled into Table 9. A typical chip can be divided into two parts: the separated portion containing the "teeth" and the continuous portion that they are connected to.

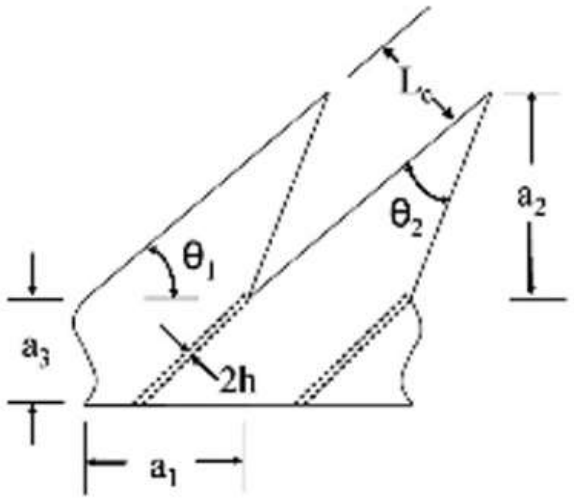

Figure 57: Chip Morphology Parameters[27]

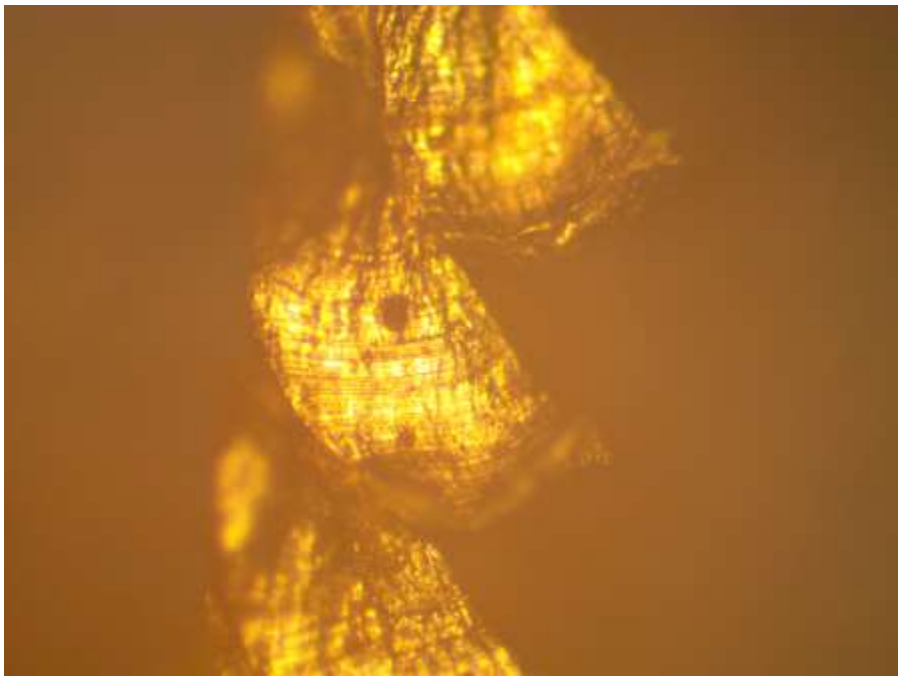

Figure 58: 10x Magnification of Ti-6Al-4V chip showing Shear bands

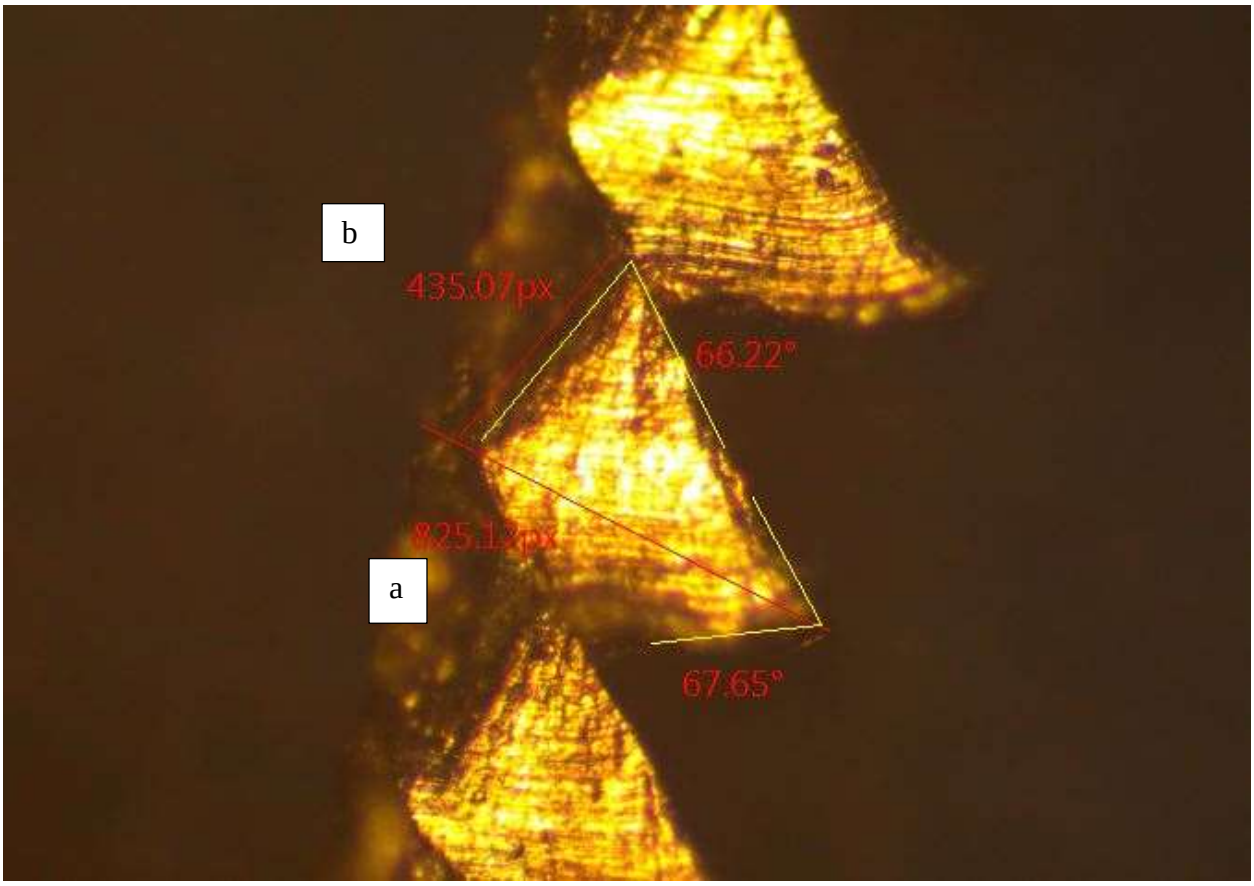

Figure 59: 10x Magnification of Ti-6Al-4V chip. Angles were measured using a metallurgical microscope; distances were calibrated by measuring the chip thickness with a micrometer, then comparing that to the average width pixel count (a), the ratio of pixels/ inch was then applied to band width (b)

	S = 9 m/min	S = 30 m/min	S = 45 m/min
f = 0.01 in / rev.			
f = 0.005 in/ rev.			

Figure 60: 10x Magnification of chips generated under different cutting conditions

Table 9: Measured chip geometries and parameter values

Run	Feed	Speed	Total Thickness $a_3 + a_2$ (.in)	Average θ_1	Average θ_2	Avg. Band Width (.in)
1	0.01	9	0.0124	41.58	40.46	0.0085
2	0.01	30	0.0120	47.29	74.07	0.0102
3	0.01	45	0.0100	49.53	60.37	0.0076
4	0.005	9	0.0052	77.71	86.04	0.0043
5	0.005	30	0.0050			
6	0.005	45	0.0052	66.20	87.76	0.0048

No Adiabatic Shear Bands were observed during Run 5

Feed rate is compared to chip thickness, θ_1, and shear band width (Fig. 61-63)

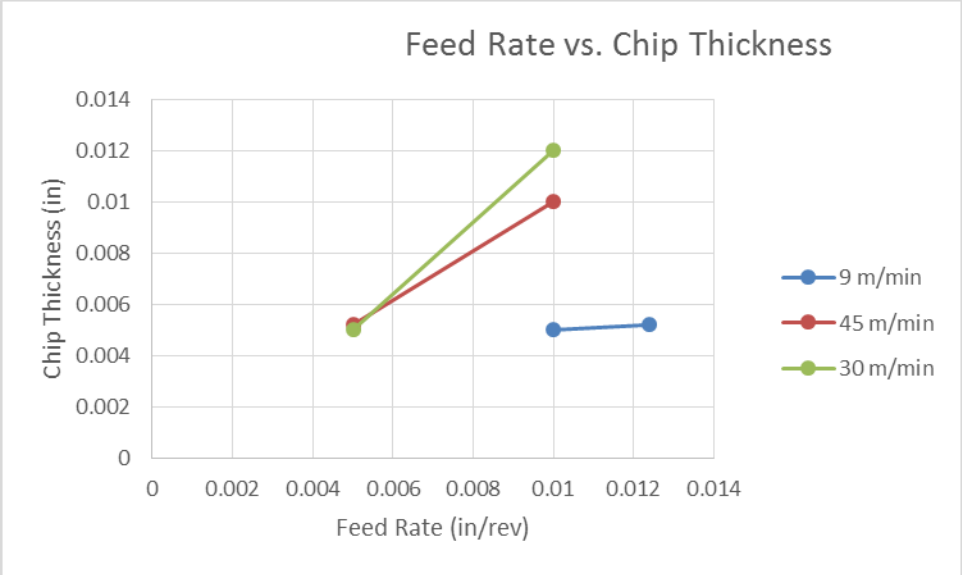

Figure 61: Feed Rate vs. Chip Thickness : While not part of the DOE, a cutting experiment was done at f = 0.02 (as seen in the graph above) this point continues the trend of previous data points.

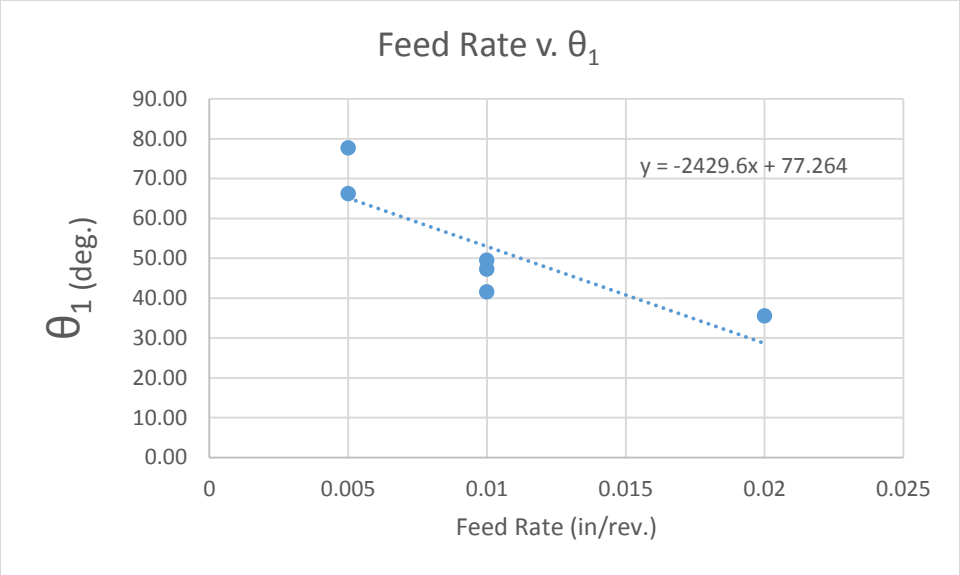

Figure 62: Feed Rate vs. Angle 1

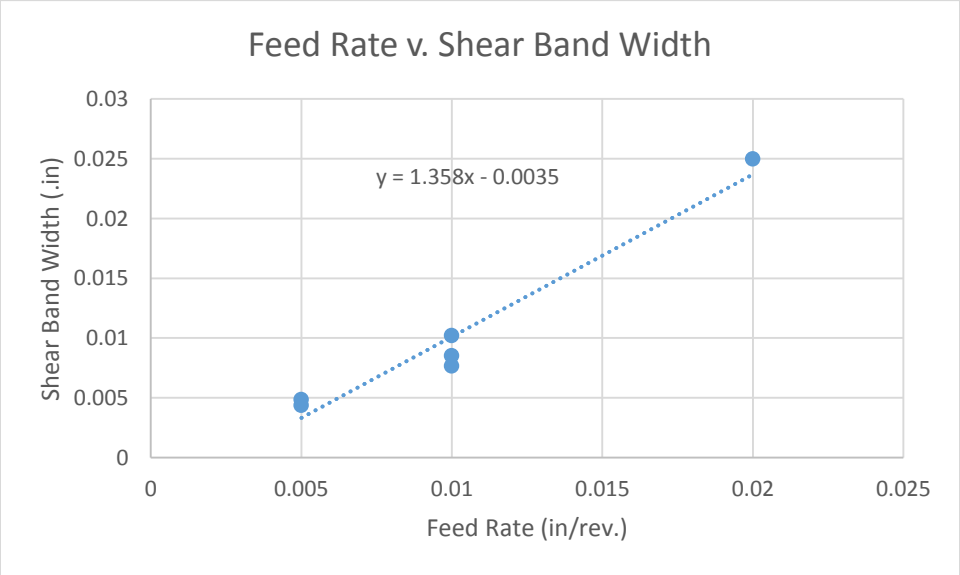

Figure 63: Feed rate vs. Shear Band Width

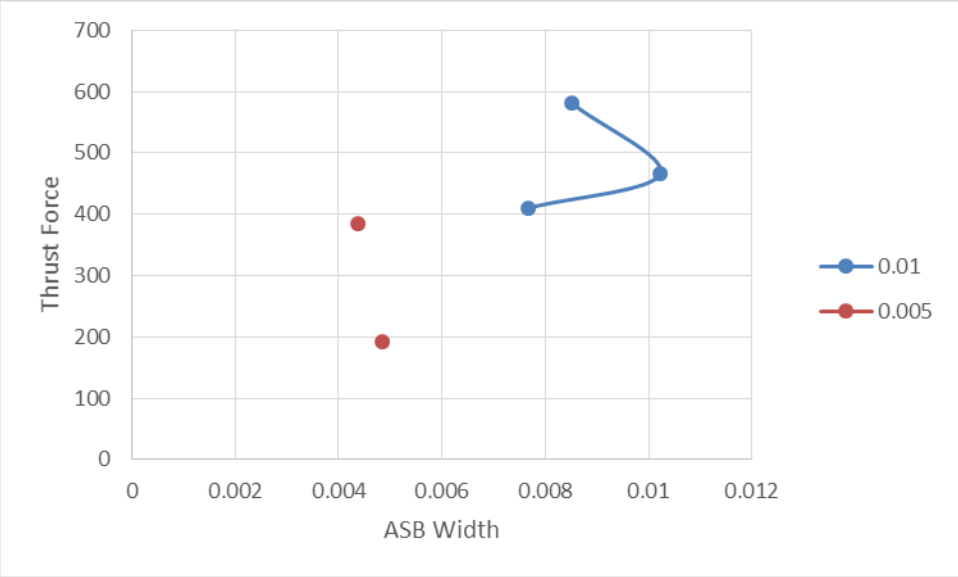

Figure 64: ASB width in relation to thrust force

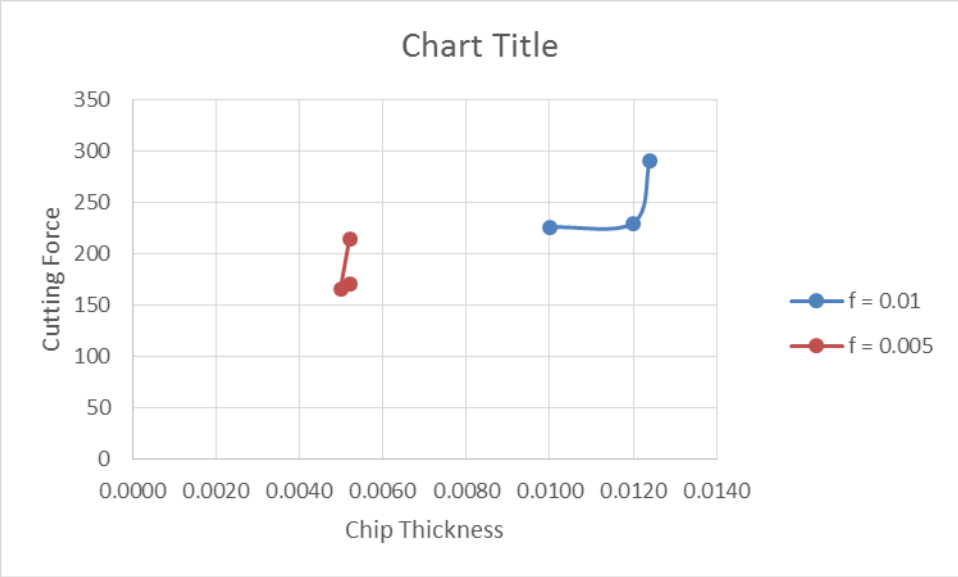

Figure 65: Chip thickness in relation to cutting force

Data Analyses, and Control of ASB-Induced Characteristics for Productivity

From the dynamometer force data plots, it can be observed that an increase in cutting speed (from 9m/min to 45 m/min) resulted in a small decrease in the cutting and thrust forces; however both the cutting and feed forces showed a marked and consistent increase with an increase in the feed rate (from 0.005 in/rev to 0.01 in/rev). This trend is consistent with the behavior of different force components in traditional machining literature.

When considering the accelerations in the thrust and cutting directions, except at the lowest surface speed (of 9 m/min), both the accelerations showed significant increases with feed rate. Though the accelerations were fairly steady at the lower feed rate (of 0.005 in/rev) regardless of surface speed, both accelerations showed a significant increase with surface speed at the higher feed rate (of 0.01 in/rev). This suggests that as the cutting conditions tend to be towards higher material removal rates, meaning at higher feeds or speeds, the accelerations seem to be becoming much more significant.

Considering chip morphology, the chip thickness increased in proportion to the feed rate consistently, and had a smaller effect from surface speeds. This is accordance to chip morphology behavior in machining literature. The ASB width also increased in proportion to the feed rate signifying that it is the primary factor controlling the ASB width, much more than surface speeds. When considering the relations between chip/ASB widths and the cutting forces, no significant trend was observed. Altogether, this leads to the conclusion that controlling feed rates will allow for ASB width control, and hence the magnitude and frequency of the force and acceleration variations during the serrated chip formation process.

CHAPTER V

CONCLUSIONS & DISCUSSIONS

This project served to investigate the ultra-high frequency aspects of adiabatic shear banding (ASB) during the Ti-6Al-4V chip generation process. For this, a piezoelectric-based dynamometer and an accelerometer was assembled and calibrated for measuring the multi-directional forces and accelerations experienced by the cutting tool during machining, and especially pertaining to the ASB process. An experimental design of machining tests based off the lower portion of the range of recommended parameters for Ti-6Al-4V turning was conducted. This helped to elucidate the relationships between ASB-induced machining force and acceleration components to the resulting chip morphology and other process characteristics. This understanding also helped generate strategies to suitably alter process parameters for improvements in productivity.

Intellectual Contributions

Some of the major conclusions that can be drawn from this study are listed below:

- It can be concluded that feed rate (as opposed to sliding velocity) has a greater effect on most chip-related dimensions (a higher feed rate generally translates to a larger chip dimension)
- Feed rate also had a greater and directly proportional relationship to machining force components. Instead, both cutting force and thrust force were observed to have inversely proportional relationships with cutting speed.

- Considering shear bands, a higher feed rate resulted in higher shear band width, and these had a direct proportionality relationship.
- Controlling feed rates will allow for ASB width control, and hence the magnitude and frequency of the force and acceleration variations during the serrated chip formation process.

REFERENCES

1. Zhu, Z., Sun, J., Li, J. & Huang, P. Investigation on the influence of tool wear upon chip morphology in end milling titanium alloy Ti6Al4V. *Int. J. Adv. Manuf. Technol.* **83,** 1477–1485 (2016).

2. Li, Z., Liu, E. L., Wang, T. Da, Li, J. & Zheng, Y. C. Experimental Investigation of Tool Wear and Chip Morphology in Turning Titanium Alloy Ti6Al4V. *Mater. Sci. Forum* **800–801,** 81–86 (2014).

3. Li, A., Zhao, J., Zhou, Y., Chen, X. & Wang, D. Experimental investigation on chip morphologies in high-speed dry milling of titanium alloy Ti-6Al-4V. *Int. J. Adv. Manuf. Technol.* **62,** 933–942 (2012).

4. Dominic, T. Modeling of tool wear and tool fracture in micromilling. (2011).

5. Molinari, A., Soldani, X. & Miguélez, M. H. Adiabatic shear banding and scaling laws in chip formation with application to cutting of Ti-6Al-4V. *J. Mech. Phys. Solids* **61,** 2331–2359 (2013).

6. Sutter, G. & List, G. Very high speed cutting of Ti-6Al-4V titanium alloy - Change in morphology and mechanism of chip formation. *Int. J. Mach. Tools Manuf.* **66,** 37–43 (2013).

7. Zhu, L., Wu, J., Li, Z. & Liu, C. Investigating chip morphology and its characteristics in the high-speed milling of a Ti-6Al-4V thin plate. *J. Mech. Sci. Technol.* **29,** 4359–4366 (2015).

8. Rubens Schatz II, Sachin Kamat, M. K. Chip Morphology Effects on the Surface Roughness & Machining Forces when Turning Ti-6Al-4V.

9. Landau, P., Venkert, A. & Rittel, D. Microstructural aspects of adiabatic shear failure in annealed Ti6Al4V. *Metall. Mater. Trans. A Phys. Metall. Mater. Sci.* **41,** 389–396 (2010).

10. Iit, M. E. Machining Dynamometers for measuring cutting.

11. Molding, I. Kistler – Your partner for efficiency and quality.

12. Liu, J., Li, M., Qin, L. & Liu, J. Principle research on a single mass piezoelectric six-degrees-of-freedom accelerometer. *Sensors (Basel).* **13,** 10844–10855 (2013).

13. Jurkõw, D., Dąbrowski, A., Golonka, L. & Zawada, T. Preliminary model and technology of piezoelectric low temperature co-fired ceramic (LTCC) uniaxial accelerometer. *Int. J. Appl. Ceram. Technol.* **10,** 395–404 (2013).

14. Tian, B., Liu, H., Yang, N., Zhao, Y. & Jiang, Z. Design of a piezoelectric accelerometer with high sensitivity and low transverse effect. *Sensors (Switzerland)* **16,** (2016).

15. Walter, P. L. The History of the Accelerometer. *Sound Vib.* 9 (2007).

16. Wagner., J. & Burgemeister, J. Piezoelectric Accelerometers. *Evaluation* (2012).

17. Serridge, M. & Licht, T. R. Accelerometers Piezoelectric and Vibration Preamplifiers. Theory and Application Handbook. 151 (1987).

18. Mel'nik, S. S., Sobolev, M. D. & Loginov, P. M. Dynamic Error of Piezoelectric Impact Accelerometers Attached to Elastic Gaskets. *Meas. Tech.* **59,** 512–515 (2016).

19. Mabrouki, T. *et al.* Some insights on the modelling of chip formation and its morphology during metal cutting operations. *Comptes Rendus - Mec.* **344,** 335–354 (2016).

20. Zheng, C. *et al.* Capturing of the propagating processes of adiabatic shear band in Ti-6Al-4V alloys under dynamic compression. *Mater. Sci. Eng. A* **658,** 60–67 (2016).

21. Molinari, A., Musquar, C. & Sutter, G. Adiabatic Shear Banding in High Speed Machining of {T}i-6{A}l-4{V}: Experiments and Modeling. *Int. J. Plast.* **18,** 443–459 (2002).

22. Kiani, M. On the Role of machining strategies on the Efficiency of Titanium Machining. (2016).

23. Thesis, A. Increasing Efficiency of Ti-6Al-4V Machining by Cryogenic Cooling and using Nanolubricants. (2016).

24. Response, W. F. & Accelerometer, V. M. K-Shear ® Accelerometer. 1–2 (2008).

25. Nationals Instruments. User guide and specifications NI USB 6008/6009. 1–23

26. Load, C. *et al.* iLoad Mini ™ Load Cell Aluminum iLoad Mini Load Cell. (2009).

27. Upadhyay, V., Jain, P. K. & Mehta, N. K. Comprehensive study of chip morphology in turning of Ti-6Al-4V. *5th Int. 26th All India Manuf. Technol. Des. Res. Conf.* 2–7 (2014).

28. Calamaz, M., Coupard, D., Nouari, M. & Girot, F. Numerical analysis of chip formation and shear localisation processes in machining the Ti-6Al-4V titanium alloy. *Int. J. Adv. Manuf. Technol.* **52,** 887–895 (2011).

APPENDIX

MATLAB Codes

Code_Mean_Filter_XYZ.m

(The code in this m-file was used to read the data from the DAQ and create comparative plots. See code comments for individual line functions.)

```
clc % clear all
clear all;
close all % close all

load Run.txt %% Name of the file to be read
SET= Run;

avgx = mean(SET(100:300,4)); %% Adjusting the DC bias to zero
avgy = mean(SET(100:300,5)); %% Adjusting the DC bias to zero
avgz = mean(SET(100:300,6)); %% Adjusting the DC bias to zero

datax = 1*(SET(:,4)-avgx); %% Sacling factor 1000, can be changes based on
the need
datay = 1*(SET(:,5)-avgy); %% Sacling factor
dataz = 1*(SET(:,6)-avgz); %% Sacling factor


%%%%%%%%%%%%%%%%%%%%%%%%%%%%%%%%%%%%%%%%%%%%%%%%%%%%%%%%%%%%%%%%%%%%%%%%%%%%%%%
%%%%%%%%%%%%%%%%%%%%%%%%%%
data = datax;

%*****************************************************
Fs = (1/.00016);       %input sampling frequency in Hz      *
L = length(data);  %input vector name "data"          *
%*****************************************************

%compute DFT (In English: takes FFT of ChosenColumn)
NFFT = 2^nextpow2(L);              %Next power of 2 from length of y
DFT = fft(data,NFFT)/L;
DFT = DFT(1:NFFT/2);
f = Fs/2*linspace(0,1,NFFT/2);      %generate frequencies from 0 to Fs/2

[FData] = MyButter(data,Fs,10,1);
m_FData = mean(FData);

calc_Avgx = m_FData;

%Plot force
figure(1);
plot(datax);
hold on;
plot(FData,'r');
```

```
%%%%%%%%%%%%%%%%%%%%%%%%%%%%%%%%%%%%%%%%%%%%%%%%%%%%%%%%%%%%%%%%%%%%%%%%%%%%%%
%%%%%%%%%%%%%%%%%%%%%%%%%%%%%%%%%%
data = datay;

%*******************************************************
Fs = 6250;       %input sampling frequency in Hz      *
L = length(data);  %input vector name "data"          *
%*******************************************************

%compute DFT (In English: takes FFT of ChosenColumn)
NFFT = 2^nextpow2(L);               %Next power of 2 from length of y
DFT = fft(data,NFFT)/L;
DFT = DFT(1:NFFT/2);
f = Fs/2*linspace(0,1,NFFT/2);      %generate frequencies from 0 to Fs/2

[FData] = MyButter(data,Fs,10,1);
m_FData = mean(FData);

calc_Avgy = m_FData;

%Plot force
figure(2);
plot(datay);
hold on;
plot(FData,'r');

%%%%%%%%%%%%%%%%%%%%%%%%%%%%%%%%%%%%%%%%%%%%%%%%%%%%%%%%%%%%%%%%%%%%%%%%%%%%%%
%%%%%%%%%%%%%%%%%%%%%%%%%%%%%%%%%%
data = dataz;

%*******************************************************
Fs = 6250;       %input sampling frequency in Hz      *
L = length(data);  %input vector name "data"          *
%*******************************************************

%compute DFT (In English: takes FFT of ChosenColumn)
NFFT = 2^nextpow2(L);               %Next power of 2 from length of y
DFT = fft(data,NFFT)/L;
DFT = DFT(1:NFFT/2);
f = Fs/2*linspace(0,1,NFFT/2);      %generate frequencies from 0 to Fs/2

[FData] = MyButter(data,Fs,10,1);
m_FData = mean(FData);

calc_Avgz = m_FData;

figure(3);
plot(dataz);
hold on;
plot(FData,'r');

%%%%%%%%%%%%%%%%%%%%%%%%%%%%%%%%%%%%%%%%%%%%%%%%%%%%%%%%%%%%%%%%%%%%%%%%%%%%%%
%%%%%%%%%%%%%%%%%%%%%%%%%%%%%%%%%%
```

```
calc_Avgx
calc_Avgy
calc_Avgz
```

MyButter.m

(This code is a subroutine used by Code_Mean_Filter_XYZ.m (above), see line comments for individual line functions)

```
function [FiltData] = MyButter(InputData,SampFreq,CutoffFreq,Order)
%Note: SampFreq and CutoffFreq should be given in Hz.  InputData
%should belong to R^n (it should be an n-dimensional vector)

% CutoffFreq = 20;
% Order = 2;

clear b a

wo = CutoffFreq/(SampFreq/2);
[b,a] = butter(Order,wo);

FiltData1=zeros(size(InputData));
for i=1:length(InputData)
    if i <= Order
        FiltData1(i) = InputData(i);
    else
        for j = 0:Order
            if j == 0
                FiltData1(i) = FiltData1(i) + b(j+1)*InputData(i-j);
            else
                FiltData1(i) = FiltData1(i) + b(j+1)*InputData(i-j) -
a(j+1)*FiltData1(i-j);
            end
        end
    end
end
FiltData = FiltData1;
```